

Improving the Characteristics of Nickel Coatings Produced on Copper from Watts Bath in the Presence of Ascorbic Acid – Combined Experimental and Theoretical Study

Manal A. El Sayed¹, Morad M. El-Hendawy², Magdy A.M. Ibrahim^{3,*}

¹ Department of Physics, College of Science and Arts, Qassim University, Al Bukairiyah, Saudi Arabia.

² Chemistry Department, Faculty of Science, New Valley University, Kharga 72511, Egypt.

³ Department of Chemistry, Faculty of Science, Ain Shams University, Abbassia, Cairo 11566, Egypt

*E-mail: imagdy1963@hotmail.com

Received: 14 October 2021 / Accepted: 30 January 2022 / Published: 4 March 2022

Ascorbic (Asc) acid as an environmentally friendly additive for nickel electrodeposition from Watts bath has been inspected. X-ray diffraction (XRD) and scanning electron microscopy (SEM) examinations were employed to assess the structure and morphology of the prepared Ni coatings. The influence of Asc acid on the current efficacy, polarization behavior, current-time transients, anodic linear stripping voltammetry, and macro-throwing power are the main points addressed in this research. Asc acid addition to the bath resulted in significant improvements in some important characteristics of the prepared Ni coatings, such as microhardness, throwing power, and corrosion resistance. The great shift of the polarization curves towards the less noble direction upon the addition of Asc acid demonstrated the inhibition of Ni deposition, which might be assigned to Asc acid adsorption on the cathode's active sites thus, delaying the rate of Ni²⁺ deposition. The data matched well with the Langmuir adsorption isotherm. The chronoamperometry study revealed that the formation of nickel nuclei is controlled by diffusion *via* a nucleation and growth mechanism. The inclusion of Asc acid into the Watts bath not only modified the texture of the formed Ni coatings, as demonstrated from XRD analysis but also produced more fine grains as shown by SEM observation. Such desirable characteristics made the prepared Ni coatings able to effectively resist both the uniform and pitting corrosion processes in NaCl solutions, as evidenced from Tafel extrapolation, linear polarization resistance (LPR), and potentiodynamic anodic polarization measurements. Computational studies based on the density functional theory (DFT) and Monte Carlo simulation revealed the formation of several nickel complexes in the bath based on the three known forms of ascorbic acid under acidic conditions. All these *in situ* generated compounds having a high tendency for adsorption on the copper surface are believed to participate in the delay of the rate of electroplating.

Keywords: Ni electrodeposition. Ascorbic acid. Uniform and pitting corrosion inhibition. Density functional theory. Monte Carlo simulation.

1. INTRODUCTION

Nickel electrodeposition is regularly used in operations of decoration, engineering, and electroforming [1,2]. In addition, to boost the appearance, nickel deposition has been a common practice for the preparation of usable layers on items to enhance their corrosion and endurance resistance. In electrodeposition operations, it is not enough to just yield layers that have a fancy look and features. The deposit must also be used to fill the base metal with a layer as nearly regular as possible in thickness (throwing power) [3]. The preferred electroplating bath depends mainly on the characteristics required. Therefore, different authors have examined the electrodeposition of nickel using various baths [4-12]. Almost all nickel baths are composed of 'Watts' formulation, particularly those used for decorative purposes because this formulation is exceedingly viewed as cost-effective and simple to control [13]. To enhance the physical and mechanical characteristics of the coating, like brightness, coarseness, thickness, strength, and corrosion resistance, additives are commonly incorporated into the plating solution. Furthermore, one of the most powerful and most used methods to improve the throwing power of electrolytic baths is to incorporate organic compounds. Moreover, it is possible to incorporate an additive into the electrolytic bath, as it is easier to operate at lower energy consumption in comparison with the pulse electrodeposition, which includes complicated parameters such as the current waveform, density, frequency, and duty cycle change to enhance the coating properties. Therefore, the impact of additives on Ni deposition based on Watts formulation has been widely investigated using various molecules such as: 2- and 4-picoline [14], 2-butyne-1,4-diol [15], thiourea [16], 1,2-benzisothiazole [17-19], monoethanolamine (MEA) [20], L-proline [8], nitrate [12], glycine [10], p-ethoxycyanothioformanilide (PECTF) [21], phytic acid [22], and natural kermes dye (NKD) [9]. Cobley et al. [23] studied the inclusion of Asc acid in copper electroplating bath utilizing catalytic anodes and found that Asc acid causes a powerful rebate of the oxidation rate of the brightener.

Independently, a method for the study of cobalt in Ni-based alloys was recommended and it was found that the harmony and aspect of the atomic absorption profiles [24] were also improved by Asc acid. The effect of pH value, temperature, current density, and Asc acid stabilizer concentration on the element content, rate of deposition, and microhardness of nickel-iron-tungsten alloy coatings was also studied by Jinku et al. [25]. It was found that upon increasing Asc acid concentration, the deposition rate of the coating declines, while the morphology of the coating surface becomes rougher. To our knowledge, no studies focused on using Asc acid as an effective additive on nickel reduction during the electrodeposition processes. The current research is therefore aimed at the formation of Ni coatings from a Watts-formulation containing Asc acid to boost the properties of nickel coatings. Furthermore, the work focuses on the kinetics of nickel deposition and the impact of Asc acid on the uniform and pitting corrosion characteristics of the as-prepared Ni coatings in NaCl solutions. Tafel extrapolation and linear polarization resistance (LPR) methods were employed to study the uniform corrosion behavior of the Ni coatings. The anodic responses (passive layer growth and breakdown) of the Ni deposits were assessed using potentiodynamic anodic polarization measurements.

The coordination chemistry of L-ascorbic acid is ambiguous due to its flexible nature of chelating to different metal ions with different geometries [26,27]. For this reason, DFT modeling was employed in the current study as a powerful tool to gain insight into the bonding interactions of the complexing

agent with Ni^{2+} ions in the nickel electroplating bath. The Monte Carlo (MC) simulation is another effective tool for studying the interactions between molecules and interfaces [28,29]. MC simulations can be utilized to simulate adsorption interactions between the complexing agent/Ni-complexes and the copper cathode surface during the electroplating process.

2. EXPERIMENTAL

Electrochemical formation of Ni coating was carried out utilizing a Ni electrolyte of the Watts-type consisting of 0.63 M of nickel sulphate hexahydrate, 0.09 M of nickel chloride hexahydrate, and 0.3 M of boric acid in the absence and presence of Asc acid at pH 3.0 and 27°C for 10 min. Full description of the deposition cell, the electrochemical setup, the various electrochemical techniques employed in this work, and characterizations of the prepared Ni coatings are depicted in *Sections S1-S5* (Supporting Information).

2.1. Computational details

DFT calculations were conducted to optimize the geometry of the possible Ni-ascorbate complexes that are expected to form in the electroplating bath between Ni^{2+} and ascorbic acid. Monte Carlo simulations were also carried out to investigate the adsorption of the nine proposed compounds (six Ni-ascorbate complexes + L-ascorbic acid and their deprotonated forms) on the substrate (Cu) surface, as fully reported in *Section S6* (Supporting Information).

3. RESULTS AND DISCUSSION

3.1. Polarization behavior

The E - j curves traced from the Watts formulation during the nickel electrodeposition in the absence and existence of various Asc acid concentrations are displayed in Fig. 1. At a scan rate of 5 mVs^{-1} , the potential was swept from -0.5 V towards more negative potential. The presence of Asc acid not only caused a significant shift in the deposition potential but also the polarization curves moved towards more negative potentials. This change became more pronounced upon increasing Asc acid concentration in the bath. This major change in the cathodic polarization curves may be ascribed to high-energy surface adsorption of Asc acid and growth site deposition, resulting in poisoning or inhibiting effect on the most active growth sites [30, 31]. In other words, Asc acid behaves like an inhibitor for Ni electrodeposition. Fig. 2 exhibits the influence of pH (2.6-3.4) on the behavior of cathodic polarization. The polarization curves were highly pH-dependent and shifted towards less noble potential values upon increasing the pH of the bath. This behavior might be due to the reduction in H_2 overpotential.

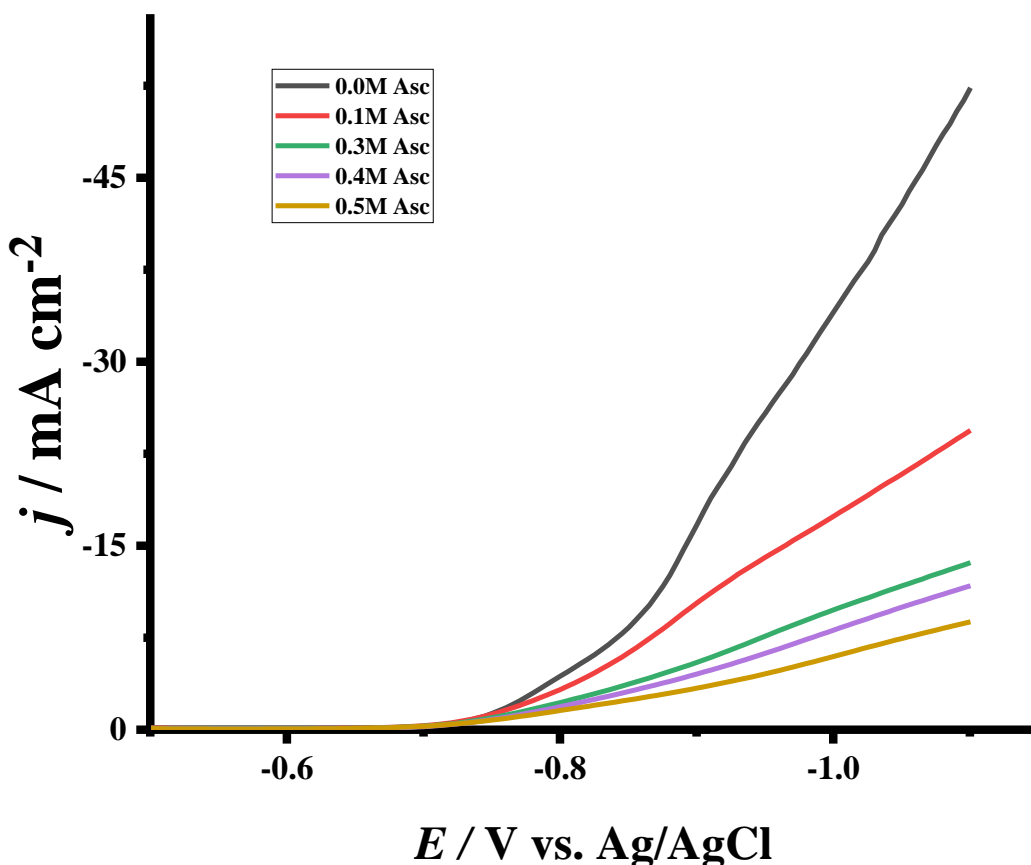


Figure 1. Polarization behavior during nickel deposition on a copper substrate from Watts bath in the absence and presence of different concentrations of Asc acid at pH 3.00 and at 27°C.

To illustrate the impact of Asc acid concentration and pH on the cathodic reduction kinetics of Ni^{2+} ions, Tafel lines were generated by plotting $\log j$ versus the cathodic polarization, as stated by Tafel equation:

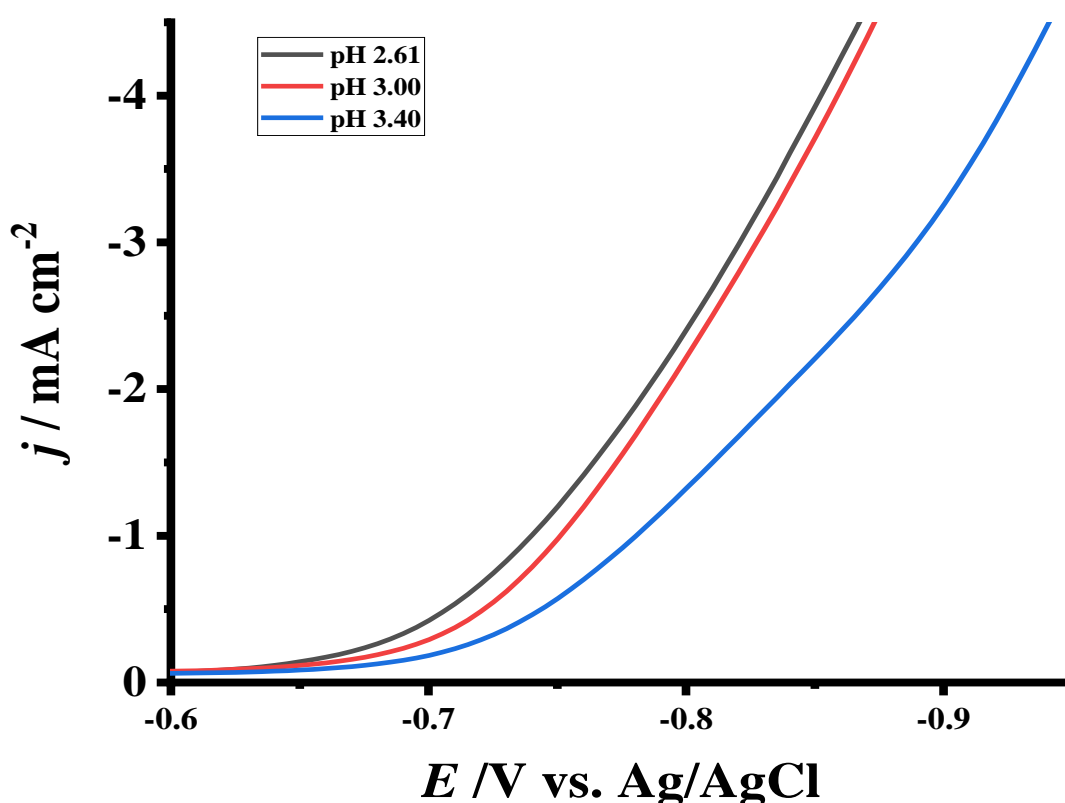
$$\eta = a + b \log j \quad (1)$$

$$b = RT/\alpha nF$$

where b is the slope of the Tafel, α is the transfer coefficient, defined as the fraction of the electrostatic potential energy that affects the reduction rate in an electrode reaction, with the corresponding oxidation rate affected by the remaining fraction $(1-\alpha)$. Exchange current densities, j_0 , for nickel deposition were obtained by extending the Tafel lines to an overpotential value equal to zero. Table 1 lists the Tafel slopes, determined from the straight lines for different Asc acid concentrations, along with the exchange current densities, j_0 , and the transfer coefficient, α .

Table 1. Tafel parameters of Ni electrodeposition from Watts-type bath at various Asc concentrations and different pH (0.4 M Asc.).

Variable	$-b$ (mV decade ⁻¹)	i_0 A cm ⁻²	A
[Asc] / M			
0.0	0.757	1.7×10^{-2}	0.0292
0.1	0.727	1.1×10^{-2}	0.0281
0.3	0.673	1.0×10^{-2}	0.0260
0.4	0.472	4.4×10^{-3}	0.0182
0.5	0.415	2.4×10^{-3}	0.0160
pH	$-b$ (mV decade ⁻¹)	i_0 A cm ⁻²	A
2.61	0.710	0.028	0.0263
3.00	0.673	0.01	0.0260
3.40	0.657	9.7×10^{-3}	0.0256

**Figure 2.** Polarization behavior during nickel deposition on a copper substrate from Watts bath at different pH values (in the presence of 0.4 M Asc.) at 27°C.

The data in Table 1 refer that both b and α decreased markedly at low Asc acid concentrations, indicating that Asc acid has strongly affected the charge transfer reaction i.e., α is regulated by the presence of Asc acid. Moreover, a significant reduction in j_0 was also observed with enhancing the Asc acid concentration. It is well-known that j_0 is reduced when the reduction is inhibited [10], implying that

the rate of Ni²⁺ ion transfer across the EDL is inhibited by Asc acid. It should be noted here that the reduction in j_o with increasing Asc acid concentration is systemic and harmonic with increased additive adsorption (Fig. 1). On the other hand, b and j_o decrease with increasing the pH, while α is nearly constant.

3.2. Adsorption isotherm

Adsorption of additives may result from electrical attraction of the charge at the cathode for an ionic agent, or for one which possesses a permanent or induced dipole (electro-sorption). On the cathode, the additive molecule (Asc acid) is expected to adsorb on the surface, leading to increased overpotential of deposition by reducing the available active Ni²⁺ ion discharge sites. It is, therefore, possible, from equation (2), to evaluate the surface coverage of the additive:

$$\theta = (1 - j_{Asc} / j) \tag{2}$$

where j and j_{Asc} are respectively the current density without and with Asc acid at -0.95V (deduced from Fig. 1). A Langmuir adsorption isotherm fits well the data, according to the following expression (3):

$$\theta / (1 - \theta) = K [C] \tag{3}$$

where K is the constant of equilibrium of the adsorption reaction and [C] corresponds to the concentration of Asc acid. The results of Langmuir plots for Asc acid adsorption data are explored in Fig. 3.

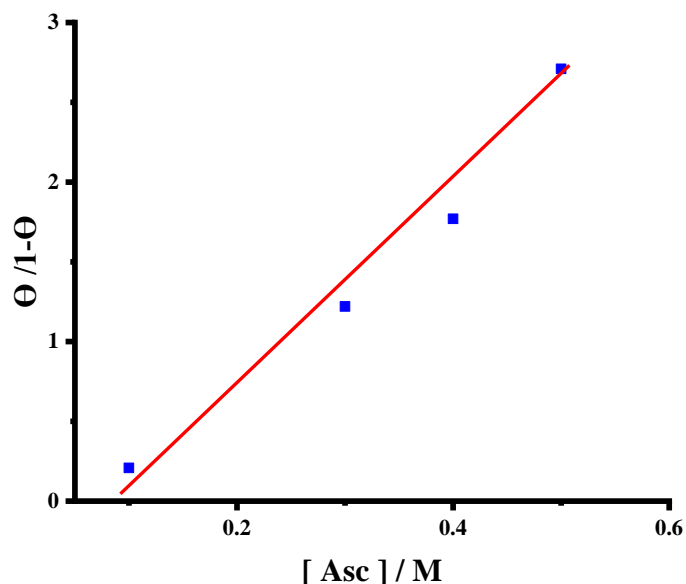


Figure 3. The plot of [Θ/(1-Θ)] vs. Asc acid concentration (deduced from Fig.1).

From the adsorption isotherm, the adsorption constant K was determined to be 5.0. Additionally, the standard free energy change (ΔG°) for adsorption was determined using equation (4):

$$\Delta G^\circ = - RT \ln (55.5 K) \tag{4}$$

where R is the general constant of gas, T is the absolute temperature and 55.5 represents the molarity of water. The calculated value of ΔG° was $-13.93 \text{ kJ mol}^{-1}$, referring that the Asc acid molecule is physically adsorbed and its negative mark points out that the inhibitor molecule interacts spontaneously with the cathode surface [32]. Electrostatic interactions between charged metal surface and molecules (physisorption) are consistent with values of ΔG° up to -20 kJ mol^{-1} , while values of ΔG° up to -40 kJ mol^{-1} or greater are correlated with chemisorption due to electron transfer/sharing between Asc acid molecules and the metal surface to form a co-ordinate bond (chemisorption) [33].

3.3. Anodic linear stripping Voltammetry (ALSV)

A set of voltammetric runs were accomplished by potentiostatic Ni deposition on Pt electrode at a constant potential value (-0.77 V) for 100 s. The potential was then moved toward the positive potentials, and without withdrawing the cathode from the solution, the stripping voltammogram was traced.

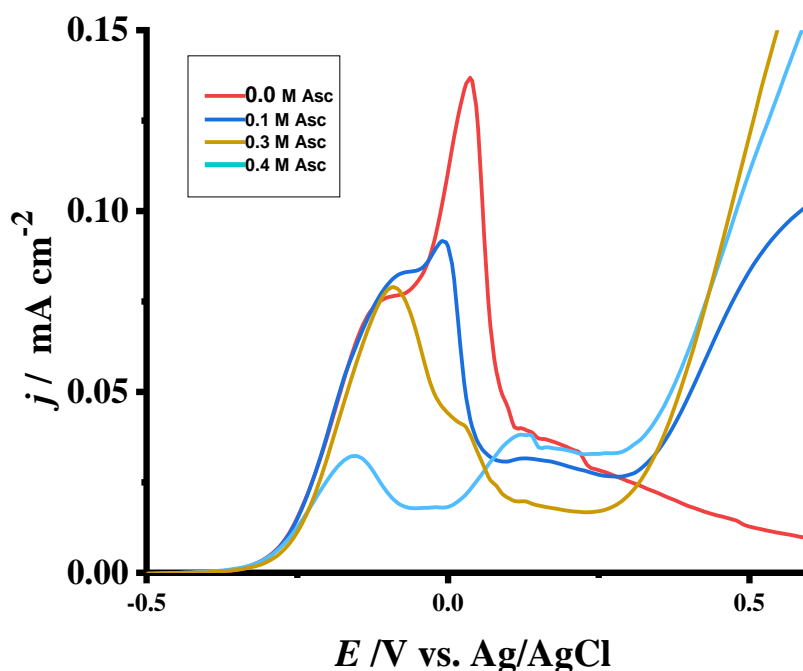


Figure 4. Anodic linear stripping voltammetric curves recorded at Pt electrode in the absence and presence of different concentrations of Asc acid at pH 3.00 and 27°C .

Fig. 4 explores the impact of the inclusion of various Asc acid concentrations. The data indicate that the peak height, as well as the region under the peak diminish with enhancing the concentration of Asc acid. This result is in line with the polarization curves presented in Fig. 1. This may be because the adsorbed Asc acid molecule, which covers the active positions, increases the cathode surface coverage. No residual Ni or NiO is seen past the stripping peak by visual inspection of the Pt surface.

Consequently, as an approximation of the quantity of deposited Ni, the charge passed through the anodic stripping peak may be accepted as a measure for the efficiency of Ni deposition. Furthermore, Fig. 5 displays the impact of pH on ALSV, revealing that upon increasing pH, the stripping charge for Ni deposition decreases, which is in good agreement with data recorded in Fig. 2.

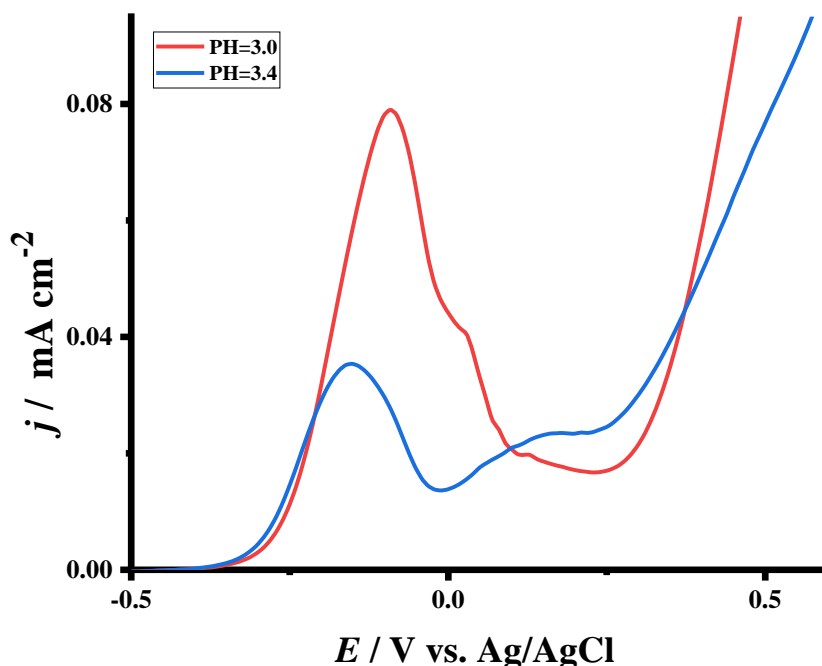


Figure 5. Anodic linear stripping voltammetric curves recorded at Pt electrode at different pH and at 27°.

3.4. Cathodic current efficiency

The current efficacy (%F) is relevant for economic reasons as it directly reflects the use of electrical energy. The impact of Asc acid concentration on the %F during Ni electrodeposition is given in Table 2. Enhancing the Asc acid concentration (0.1 to 0.4 M) was found to decrease the %F from 93.0% to 71.7%. Since rising the concentration of Asc acid contributes to its high adsorption on the cathode surface and inhibits the reduction of the Ni²⁺ ions.

Table 2. Effect of Asc concentration, current density, and temperature on %F of nickel deposition.

M] / Asc[F%	i / mAcm⁻²	F%	Temp. /°C	F %
0.0	93.0	6.9	64.3	27	85.1
0.1	87.3	13.7	85.1	37	83.0
0.3	85.1	20.6	85.5	47	82.0
0.4	71.7	27.4	86.7	57	73.6

As presented in Table 2, the impact of applied current (6.9 to 27.4 mA cm⁻²) on the %F was examined during Ni electrodeposition in presence of Asc acid. The %F increased from 64.3% to 86.7%

by raising the current density from 6.9 to 27.4 mA cm⁻². Furthermore, elevating the bath temperature from 27°C to 57°C decreases the %F from 85.1% to 73.8%. It should be noted that in industrial production, high efficacy at low temperatures can be regarded as merit.

3.5. Chronoamperometry measurements

Chronoamperometric (current-time transient) studies have been performed to earn more awareness of the initial nucleation and growth processes of Ni deposition. During the Ni²⁺ ion reduction in the absence and existence of Asc acid at E_d = -0.77 V, the current-time transients presented in Fig. 6 were traced. With time, the current-time curves display a monotonic decrease in current. The decline in the cathodic current is ascribed to the electrical double layer charging [34]. Fig. 7 depicts the current-time relationship at distinct cathodic step potential. The values of the instantaneous current decrease when the cathodic step potential is rendered more negative. For the descending portions of the current transients (deduced from Fig. 6), drawing the relationship between the current density *j* and *t*^{-1/2} reveals straight lines (insets of Figs. 6 and 7).

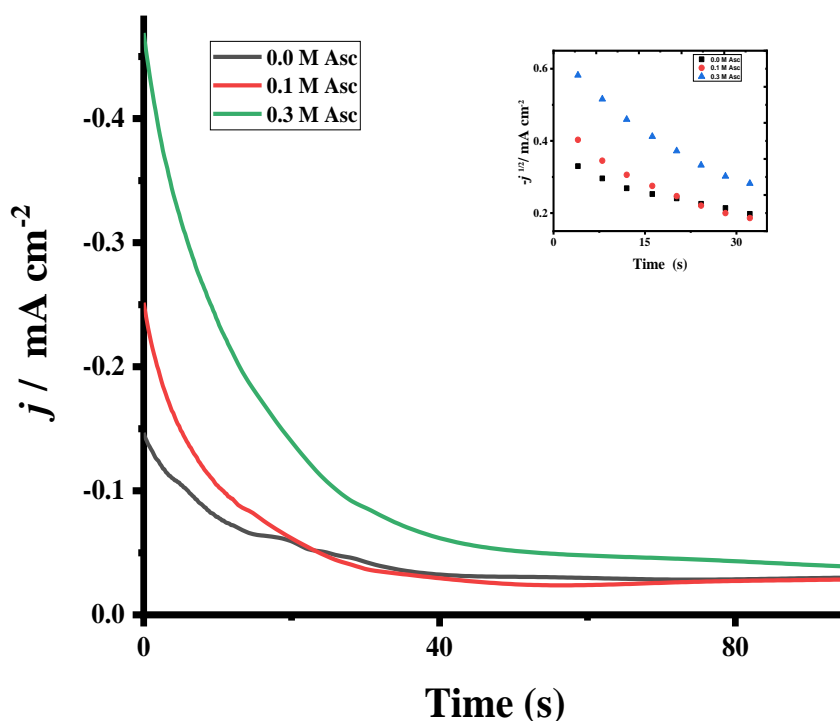


Figure 6. Potentiostatic current – time transient for nickel deposition from Watts bath recorded at Pt disc electrode in the absence and presence of different concentrations of Asc acid at a deposition potential of - 0.77 V.

The lines' slopes depend on the Asc acid concentration. This linear relation confirms the assumption that under this condition, nickel growth is a diffusion-controlled operation and follows equation (5):

$$j = P / t^{1/2} \tag{5}$$

where $P = zFcD^{1/2} / \pi^{1/2}$

where z corresponds to the number of exchanged electrons, c represents the concentration, and D is the diffusion coefficient of the diffusing species. It may be suggested that, through a nucleation and growth process, Ni deposition occurs under diffusion regulation.

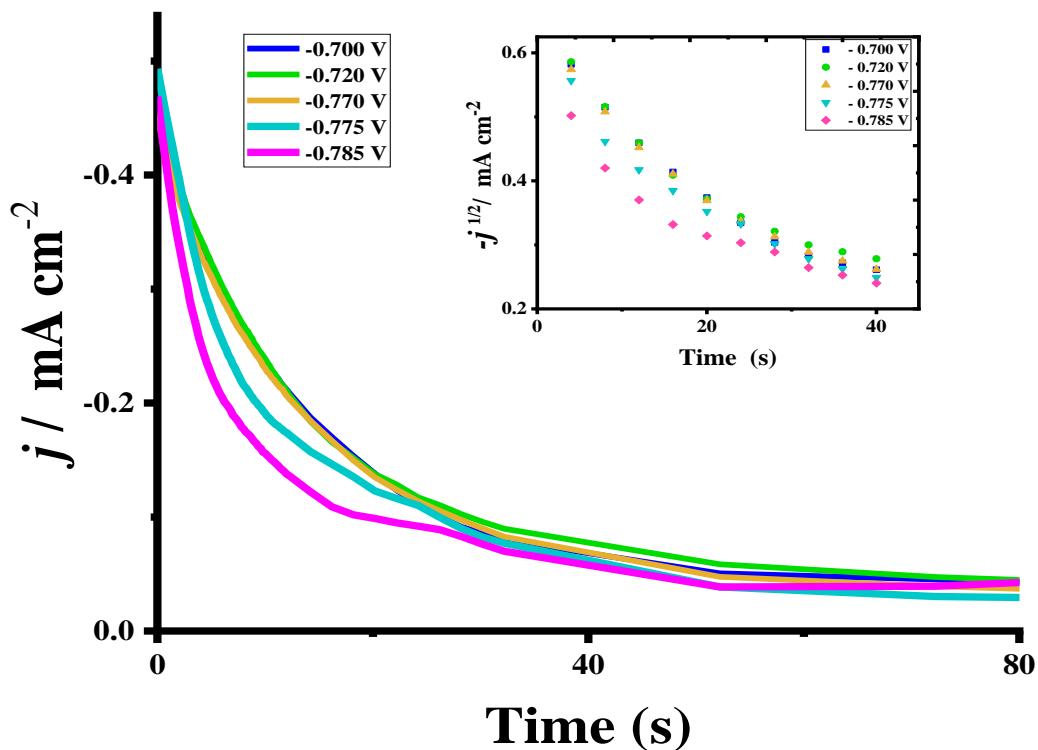


Figure 7. Potentiostatic current – time transient for nickel deposition from Watts bath recorded at Pt disc electrode in the presence of Asc acid at different deposition potential.

3.6. Throwing power

Throwing power reflects the degree to which, in absence of cathodic polarization and efficiency effects, a solution may generate deposits that are more uniform than those that would be formed under polarization. The addition of organic compounds to the plating electrolyte is one of the most efficient and commonly utilized techniques to boost both the deposit consistency and the throwing power (T.P.) of the bath [35]. The T.P. values of the Watts formulation in the absence and existence of Asc acid at 13.7 mA cm⁻² and 27°C, determined by Field’s formula at a distance proportion of 1:5, were calculated.

Table 3 reveals that the T.P. is greatly improved upon enhancement of Asc acid concentration. For example, in absence of Asc acid, the T.P.% was 2.65%, and reached 16.82% in presence of 0.4 M Asc acid, demonstrating the ability of Asc acid to improve the Watts bath T.P. The T.P.% increased more than 8 times in 0.4 M Asc acid solution.

Table 3. Effect of Asc concentration, temperature, and current density on T.P.% and T.I.

Variable	T.P.%	T.I.
[Asc] / M		
0.0	2.65	1.15
0.1	6.57	1.27
0.3	11.73	1.44
0.4	16.82	1.48
Temp./ K		
300	11.73	1.44
320	17.65	1.67
Current density mAcm ⁻²		
3.4	2.92	1.37
6.9	11.73	1.44
13.7	20.00	1.64

The improvement in throwing power may be due to Asc acid preferential adsorption on active locations. Raising the bath temperature from 27°C to 47°C leads to a large increase in throwing power, which can be caused by an increase in conductivity as the temperature rises. On the other side, there is an obvious effect on T.P. by rising the current since its value increases more than five times upon increasing the current density from 3.4 to 20.5 mA cm⁻². The results are presented in the form of throwing index (T.I.) instead of T. P. since five experimental points are given during the measurements of T. I., which minimizes errors in the calculation of any single point (see Fig. 8). Table 3 indicates that the calculated T.I. values shift at the same time as those calculated for T.P.

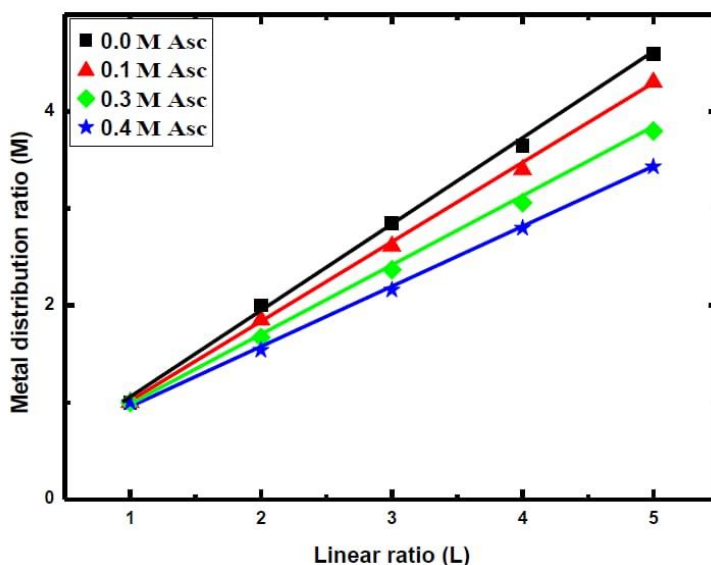


Figure 8. Metal distribution ratio M versus the linear ratio L in the absence and presence of different concentrations of Asc acid.

3.7. X-ray diffraction analysis

Table 4. The peak parameters as obtained from the X'pert HighScore Plus program and calculated lattice parameters and crystallite size for the phases of the Cu substrate (S1) and Ni-coatings (S2-S4).

		Cu					Ni				
	(hkl)	2θ (°)	β (°)	d (Å)	a (Å)	D (nm)	2θ (°)	β (°)	d (Å)	a (Å)	D (nm)
S1	111	43.186	0.332	2.093	3.625	258	44.339	0.409	2.041	3.536	210
	200	50.359	0.273	1.811	3.621	322	51.728	0.344	1.766	3.532	257
	220	74.043	0.270	1.279	3.618	369	76.303	0.337	1.247	3.527	300
	Average				3.622	316				3.531	256
S2	111	43.238	0.284	2.091	3.621	301	44.435	0.327	2.037	3.528	263
	200	50.376	0.291	1.810	3.620	303	51.806	0.345	1.763	3.527	256
	220	74.081	0.279	1.279	3.617	357	76.311	0.493	1.247	3.527	205
	Average				3.619	320				3.527	241
S3	111	43.230	0.303	2.091	3.622	283	44.408	0.398	2.038	3.531	216
	200	50.365	0.313	1.810	3.621	281	51.787	0.415	1.764	3.528	213
	220	74.074	0.311	1.279	3.617	321	76.343	0.364	1.246	3.525	278
	Average				3.620	295				3.528	236
S4	111	43.251	0.298	2.090	3.620	288	44.459	0.346	2.036	3.527	249
	200	50.378	0.331	1.810	3.620	266	51.838	0.388	1.762	3.525	228
	220	74.054	0.386	1.279	3.618	258	76.356	0.541	1.246	3.525	187
	Average				3.619	270				3.525	221

Fig. 9 displays the X-ray diffraction analysis of the as-deposited Ni (27°C , $j = 13.7 \text{ mA cm}^{-2}$, $t = 10 \text{ min}$, $\text{pH}=3.0$) from the Watts bath in the absence (S1) and presence of Asc acid at various concentrations (ca. 0.1, 0.3, and 0.4 M for S2, S3, and S4, respectively). The X'pert HighScore Plus program (PANalytical, The Netherlands) was employed to perform a whole powder pattern fitting (WPPF) of the XRD pattern of the samples S1, S2, S3, and S4 [36]. This gives accurate peak parameters such as peak position (2θ), d-spacing (d), breadth (β), etc. The obtained peak parameters are quoted in Table 4, while both the observed and calculated patterns are plotted in Fig. 9 for all four samples. Also, HighScore calculates the contributions coming from $K\alpha_2$ ($\lambda = 1.54439 \text{ \AA}$) radiation to each peak and subtracts them away, then yielding the parameters of each diffraction peak resulting only from $K\alpha_1$ ($\lambda = 1.54056 \text{ \AA}$) radiation. It is worth noting that the XRD patterns contain only the (111), (200), and (220) peaks arising from the Cu substrate and Ni phases since both share the same face-centered cubic (fcc) structure (ICDD 00-004-0850), with the substrate's lattice parameter being larger than that of Ni.

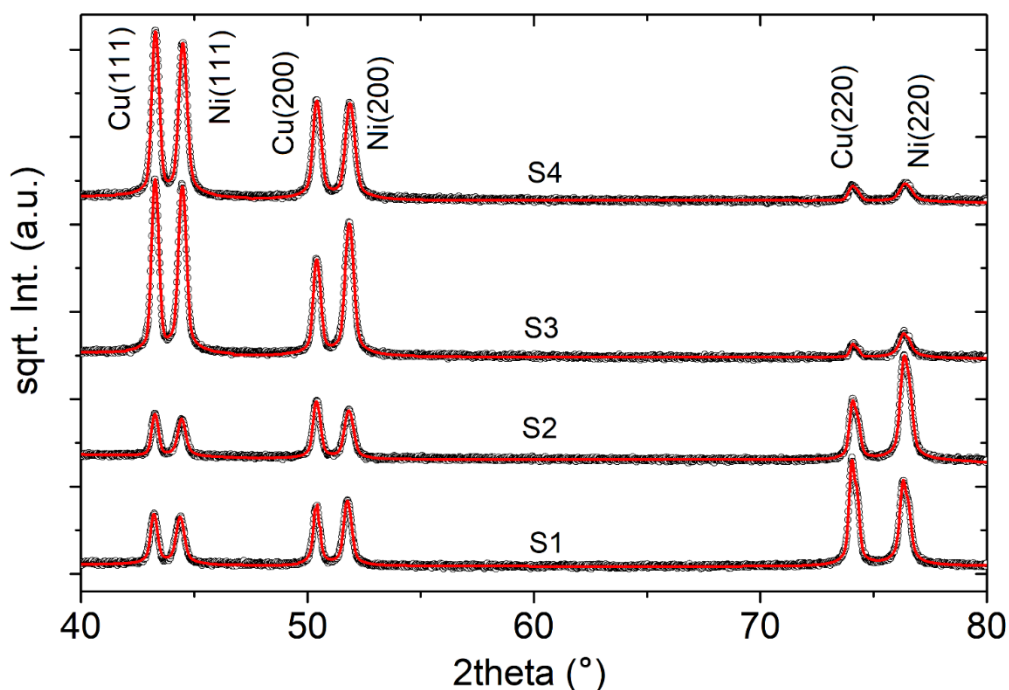


Figure 9. The XRD diffraction patterns of samples S1, S2, S3, and S4. The black circles are the observed data and the red solid line is the fitted pattern, as obtained from the X'pert HighScore Plus program. S1: Ni-coating formed without Asc acid, S2, S3, and S4: Ni-coatings formed in the presence of 0.1, 0.3, and 0.4 M Asc acid, respectively. Conditions of Ni electrodeposition (27°C , $j = 13.7 \text{ mA cm}^{-2}$, $t = 10 \text{ min}$, $\text{pH}=3.0$).

The d-spacing values of the diffraction peaks for each phase were used to calculate the lattice parameter of Cu and Ni using $a = d_{hkl}\sqrt{h^2 + k^2 + l^2}$ [33, 34] since both phases have cubic lattices. The obtained three values of the lattice parameter were then averaged and listed in Table 4. The well-known Scherrer equation $D = k\lambda/\beta\cos(\theta)$ [37, 38] was applied to estimate the crystallite-size D , a typical value of about 0.9 was assumed for the shape factor k . The average was then calculated for the three values obtained from the three peaks observed for both Cu and Ni.

The addition of Asc acid to the electroplating solution increased the intensity of the (111) Ni plane while that of the (220) Ni plane is greatly reduced. In other words, in the presence of Asc acid, the XRD patterns reflect changes in the Ni coatings' microstructure thus, referring to changes in the growth mode, and hence the texture of the nickel deposit. These changes in the deposit's microstructure take place in an Asc acid concentration-dependent manner. This is evident from the decrease in the average crystallite-size (D) values with an increase in the concentration of Asc acid, Table 4. The competitive adsorption between the Asc acid molecules and Ni^{2+} species on the Cu substrate surface, in addition to the possible complexation of Ni^{2+} by Asc acid as evidenced from theoretical studies (see later, section 3.9), and the subsequent retardation in the rate of Ni^{2+} deposition, maybe the main reasons behind such structural modifications of the nickel crystallites.

3.8. Surface morphology

Scanning electron microscopy (SEM) was acquired to assess the morphology of Ni films deposited from Asc acid-containing and Asc acid-free electrolytes and the findings are shown in Fig. 10. As it is expected, the Ni deposited from the Watts bath produces milky-like grains [21,39,40] (Fig. 10a). However, the addition of 0.3M Asc acid to the plating electrolyte leads to the production of fine circular grains filling the entire cathode surface (Fig. 10b).

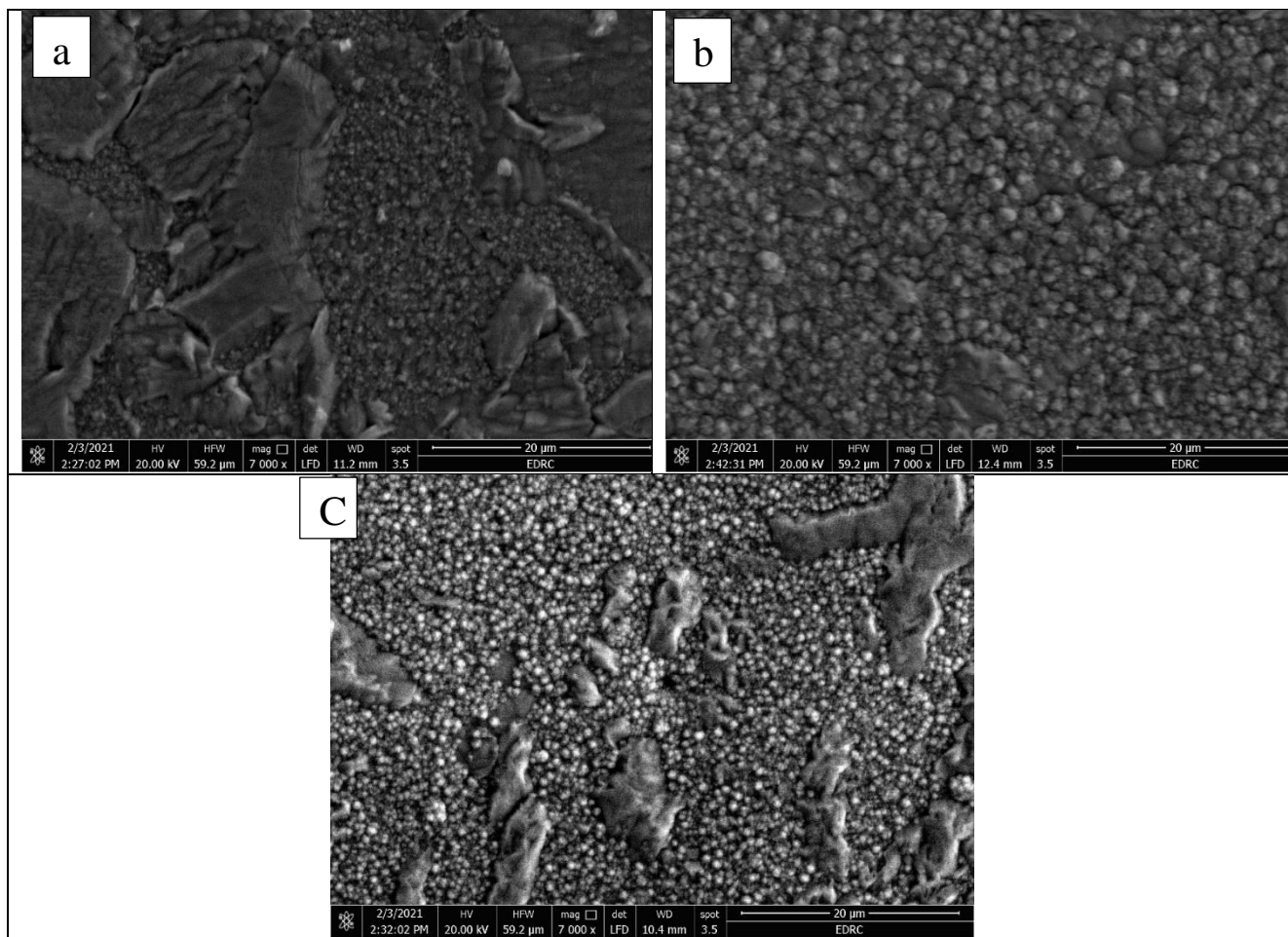


Figure 10. Scanning electron microscope images of Ni deposited from Watts-type bath in the absence (a) and in the presence of 0.3 M Asc (b) and 0.4 M Asc acid (c).

Moreover, increasing the concentration of Asc acid to 0.4 M yields finer grains (Fig. 10C). The fine grains, obtained in the presence of Asc acid, could be due to the inhibition explained clearly from the increase in the polarization (see Fig. 1). Inhibition of deposition (decrease of appropriate deposition rate, or increase of polarization) can occur through several mechanisms: decrease in the area available for electron transfer, with consequent increase of ‘true’ current density over apparent current density and concomitant increase in polarization; hindrance of surface diffusion of adions, which have not yet found sites in the growing lattice; or blockage of growth steps leading to increased concentration of adions

with increased polarization or reduced current density. Such impacts increase the production of new crystal nuclei on the metal surface and inhibit the growth of existing crystallites, resulting in a finer crystal structure result.

3.9. Microhardness of nickel coatings

Hardness measurements are commonly used in the research and development of the mechanical properties of metals and alloys and their deformation. Hardness may be defined as the resistance provided to external mechanical action by a given material attempting to scratch, abrade, indent, or otherwise affect its surface [41]. The load applied was balanced to diminish the substrate impact on the hardness values and to limit the penetration depth [42]. The Vickers microhardness, H_v of some as-deposited nickel coatings from Watts bath ($j = 13.7 \text{ mA cm}^{-2}$, 27°C , $t = 60 \text{ min.}$), was compared with that resulting from Asc acid-containing baths (Table 5).

Table 5. The microhardness of nickel films deposited from Watts bath at different concentrations of Asc.

[Asc] / M	$H_v / \text{kg f mm}^{-2}$
0.00	150
0.1	185
0.3	230
0.4	290

The findings point out that the microhardness of Asc acid-containing Ni coatings is improved compared to that of nickel deposited without Asc acid. It was found that microhardness increases from 150 kg f mm^{-2} in the absence of Asc acid to 185 kg f mm^{-2} in the 0.1 M Asc acid-containing bath. Further increase in Asc acid concentration leads to a high increase in the microhardness values. For example, raising the concentration of Asc acid from 0.1 M to 0.4 M enhances the microhardness value from 185 to 290 kg f mm^{-2} . In Asc acid solution, the possible cause of the rise in H_v may be attributable to the increased incorporation of some Asc acid moieties into the coating.

3.10. Computational study

DFT investigation

In this section, we will focus on exploring the chemical events expected to occur on the substrate (Cu) surface as well as in the plating bath. Now, we have a half cell containing a copper electrode immersed in an aqueous medium comprising the Ni^{2+} ions. The addition of L-ascorbic acid to this bath is expected to lead to several events that ultimately delay the rate of the nickel electroplating process. A recent combined experimental and theoretical study reported the possibility of formation of nine different Ni-ascorbate complexes [43].

Table 6. Some geometry information of Ni-ascorbate complexes.

	Molecular formula	M:L ratio	C.N.	Geometry	Binding mode of Asc.
1	$[\text{Ni}(\text{HA})(\text{H}_2\text{O})_4]^+$	1:1	6	Octahedral	Monodentate
2	$[\text{Ni}(\text{A})(\text{H}_2\text{O})_4]$	1:1	6	Octahedral	Bidentate
3	$[\text{Ni}(\text{A})_2]^{2-}$	1:2	4	Tetrahedral	Bidentate
4	$[\text{Ni}(\text{A})_3(\text{H}_2\text{O})_2]^{4-}$	1:3	5	Bipyramidal trigonal	Monodentate
5	$[\text{Ni}(\text{A})_3(\text{H}_2\text{O})]^{4-}$	1:3	6	Octahedral	2 Bidentate + 1 Monodentate
6	$[\text{Ni}(\text{A})_3]^{4-}$	1:3	4	Square pyramidal	2 Bidentate + 1 Monodentate

Based on our experimental conditions (pH 3), the nine complexes will be limited to only six ones, Table 6. Logically, in an acidic environment, the availability of a free hydroxyl ion is not guaranteed, therefore, we did not consider the Ni-complexes containing hydroxyl ligand.

Although Asc acid has three kinds of hydroxyl groups, vinyl OH, alcoholic-OH and carboxylic OH groups, only the vinyl OH group participates in deprotonation equilibrium and then takes part primarily in the complex formation reaction either through two vicinal oxygen centers or at least one of them [44]. Besides, Mahata et al. [44] reported that in the pH range (2.0–5.0), the neutral and deprotonated forms of Asc acid remain as H_2A , HA^- and A^{2-} , (where, HA^- and A^{2-} are monodentate and bidentate forms, respectively), Scheme 1.

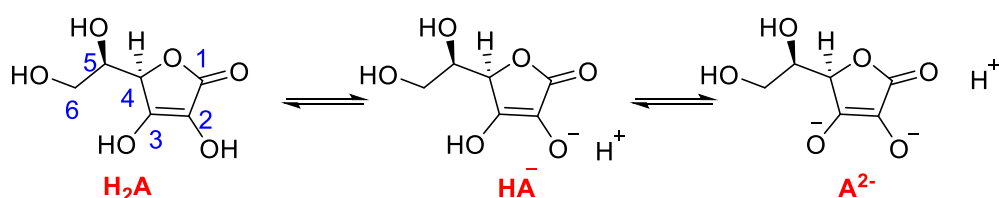
**Scheme 1.** Molecular structure of L-ascorbic acid and its protonated forms.

Table 6 summarizes the most important geometrical data of the proposed Ni-ascorbate complexes obtained from the DFT geometry optimization by M06 functional. The findings are consistent with those described by Cesario and coworkers [26]. The Cartesian coordinates of the complexes are listed in Section S7 (Supplementary Information).

Table 7. Global chemical descriptors of the studied molecules.

molecule	I_v (eV)	A_v (eV)	DM (Debye)	χ (eV)	η (eV)	ω (eV)	ΔN (eV)
H₂A	9.15	-0.30	4.50	4.42	4.72	2.07	0.01
HA⁻	9.21	2.27	5.50	5.74	3.47	4.74	-0.18
A²⁻	9.63	1.90	6.18	5.77	3.87	4.30	-0.17
1	11.43	4.66	15.14	8.04	3.39	9.55	-0.53
2	7.12	0.68	10.13	3.90	3.22	2.36	0.09
3	0.52	-4.25	4.30	-1.86	2.39	0.73	1.33
4	-32.44	15.38	131.94	-8.53	-23.91	-1.52	-0.27
5	-4.86	-11.07	11.20	-7.97	3.10	10.22	2.0
6	-5.11	-10.93	29.74	-8.02	2.91	11.04	2.15

To highlight the difference in the chemical activity of Asc acid and its complexes, we computed several quantitative chemical descriptors based on vertical ionization energy (I_v) and vertical electron affinity (A_v), Table 7. These descriptors are overall electronegativity (χ), chemical hardness (η) and electrophilicity index (ω), and the number of transferred electrons (ΔN). The details about mathematical equations used to derive the above descriptors are previously reported in the literature [43].

Electrophilicity index (ω) signifies the stability of a species by accepting a spare electron from its chemical environment. A molecule with a high ω value is a good electrophile otherwise it can be described as a nucleophile. For instance, the deprotonation of Asc acid increases the ω value. Also, the strength of electrophilicity of Ni-complexes follows the order of $6 > 5 > 1 > 2 > 3 > 4$. Global chemical hardness (η) is a direct measure of the deformation of the electron density and, hence, of the chemical reactivity [44-46]. Accordingly, the adsorption usually occurs at the region of the molecule where η has the lowest value [44]. It is noticed that deprotonation of Asc acid reduced the molecular hardness by removing nuclei from the molecule and leaving an excess negative charge on the oxygen atoms. Further, the complexation reduces the hardness steadily.

In general, the molecular dipole moment of ligands increases upon Ni-complexation, and this can enhance dipole-dipole interactions between the molecules and charged metal surface, thus favoring the adsorption process [47, 48]. The number of transferred electrons (ΔN) is given by the following equation [49]:

$$\Delta N = \frac{4.48 - \chi_{mol}}{2\eta_{mol}}$$

where χ_{mol} and η_{mol} are the absolute electronegativity and hardness of a molecule, respectively. The theoretical values are $\chi_{Cu} = 4.48$ eV/mol and $\eta_{Cu} = 0$ eV/mol [50]. The negative value of ΔN refers to the capacity of species to accept electrons. Since the electronegativity increases by deprotonation the amount of electron transfer from the metal to the ascorbate species increases, Table 7. The amount of electron transfer from the nickel species to the surface is expected to follow this order $6 > 5 > 3 > 2$. In

contrast, the ΔN of complexes 1 & 4 have negative values, so they can accept an electron from the surface.

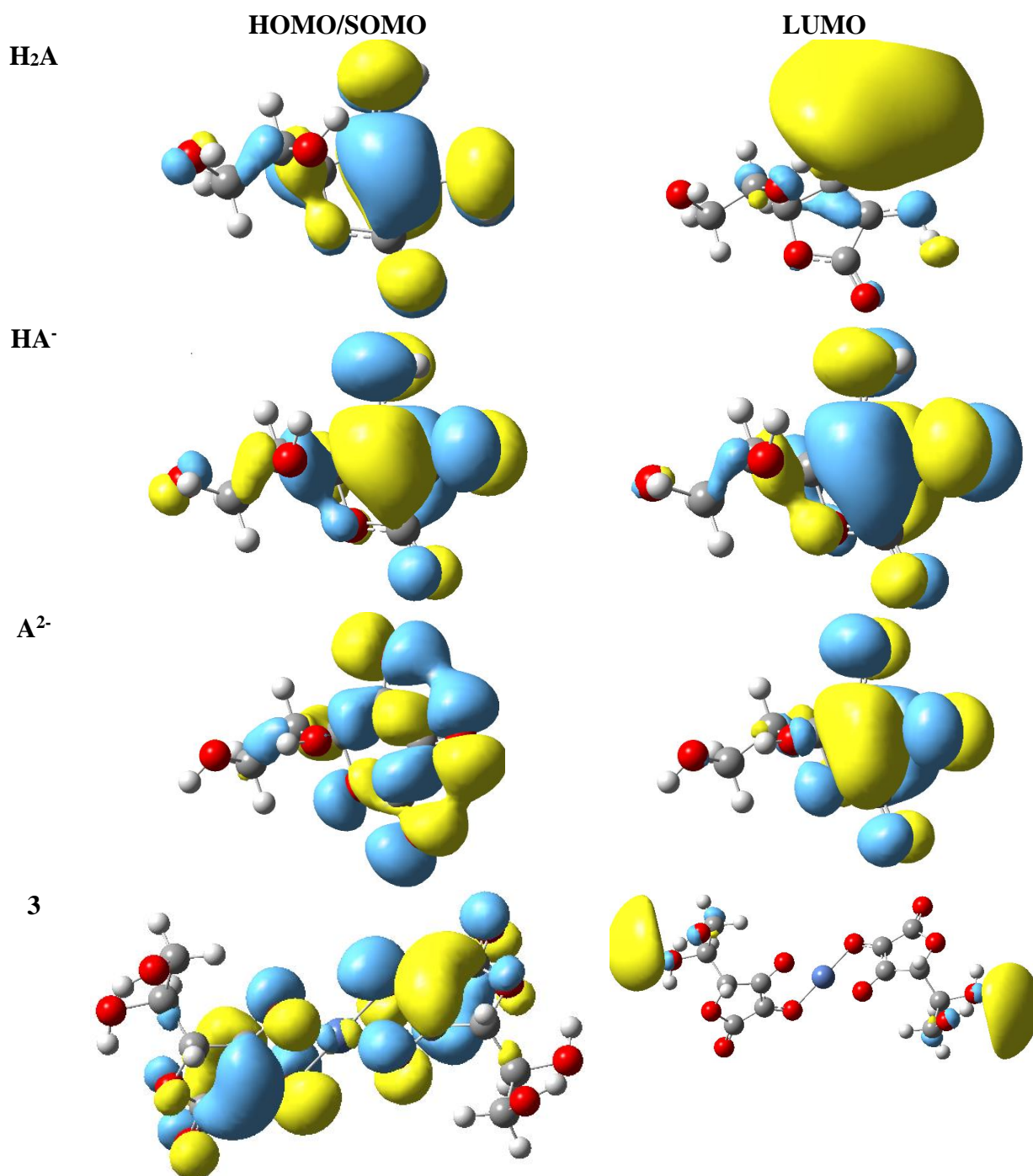


Figure 11. Frontier molecule orbital density distributions of ascorbic acid and its deprotonated forms and complex 3.

The electron density distributions of HOMO/SOMO and LUMO for Asc acid and its deprotonated forms are illustrated in Fig. 11. It is shown that the HOMO/SOMO and LUMO electron

density of the studied compounds is widely distributed over the molecular skeleton especially the furanone ring, indicating their ability to donate and accept electrons from metallic species under favorable conditions.

It turns out that, after successive deprotonation of both the vinyl hydroxyl groups, it forms a stable π -region by resonance, an electron-rich reactive region that reveals five-atom chelation with metallic ions.

The other hydroxyl groups on the side chain are not particularly dissociated in the working pH range (3.5) because they do not primarily contribute to the formation of HOMO and LUMO. Moreover, the enediol structure is stabilized by the resonance as a consequence of tautomerism with the adjacent carbonyl. This may be responsible for the adsorption of molecules on the surface of the copper as well as its complexation with Ni ions. On the other hand, the single occupied molecular orbital (SOMO) of 3 is highly localized on the furanone rings. Thus, this part is expected to share in the adsorption on the copper surface. The electron density distribution of LUMO is localized only on the chain groups.

3.11. MC simulations

The interaction energies and the adsorption modes of the three forms of Asc acid and their possible nickel complexes on the copper surface were investigated by conducting MC simulations.

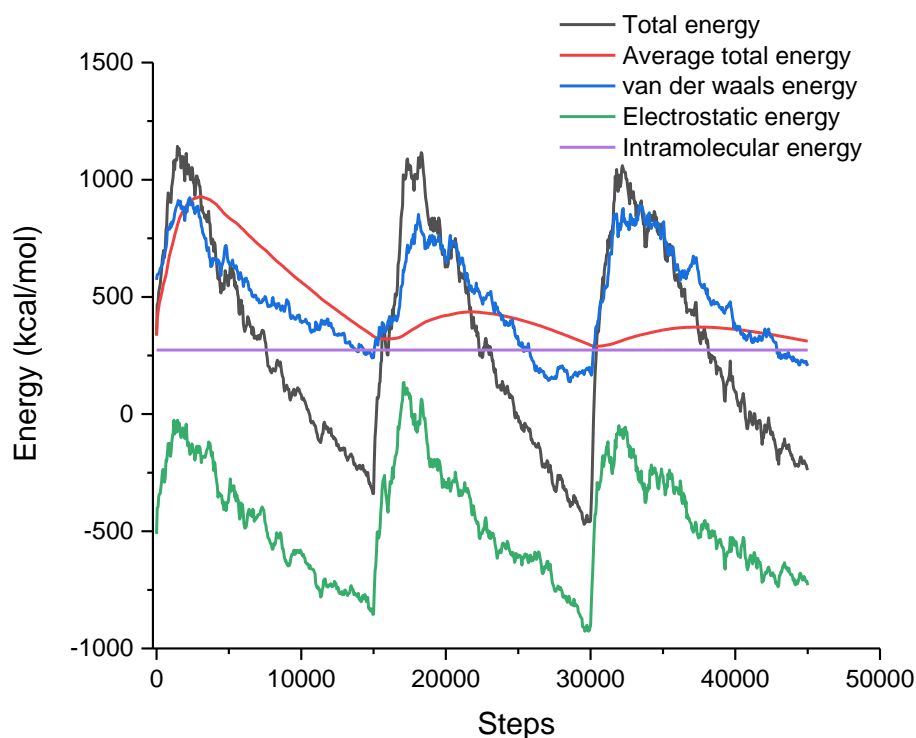


Figure 12. The different kinds of energy involved in the adsorption Cu(111)/200H₂O system in the aqueous phase during the energy optimization process by MC simulation.

In this algorithm, the best adsorption configurations for certain species were obtained through iterative rotation and translation according to certain parameters until the total energy reaches its minimum value. The total energy distribution for Cu(111)/1/2NaCl/200H₂O complex in the aqueous phase is displayed in Fig. 12 as a representative example. van der Waals energy and intramolecular energy are the main components of the adsorption process.

The most stable adsorption mode on the copper surface for H₂A, HA⁻, and A²⁻ are shown graphically in Fig. 13. The upright configuration of the furanone ring, observed of all species, can help the formation of the chelate ring with the copper surface especially in the case of A²⁻ species. Besides, adsorption of the species through the donation of lone pair of oxygen atoms depends on the nature of the species.

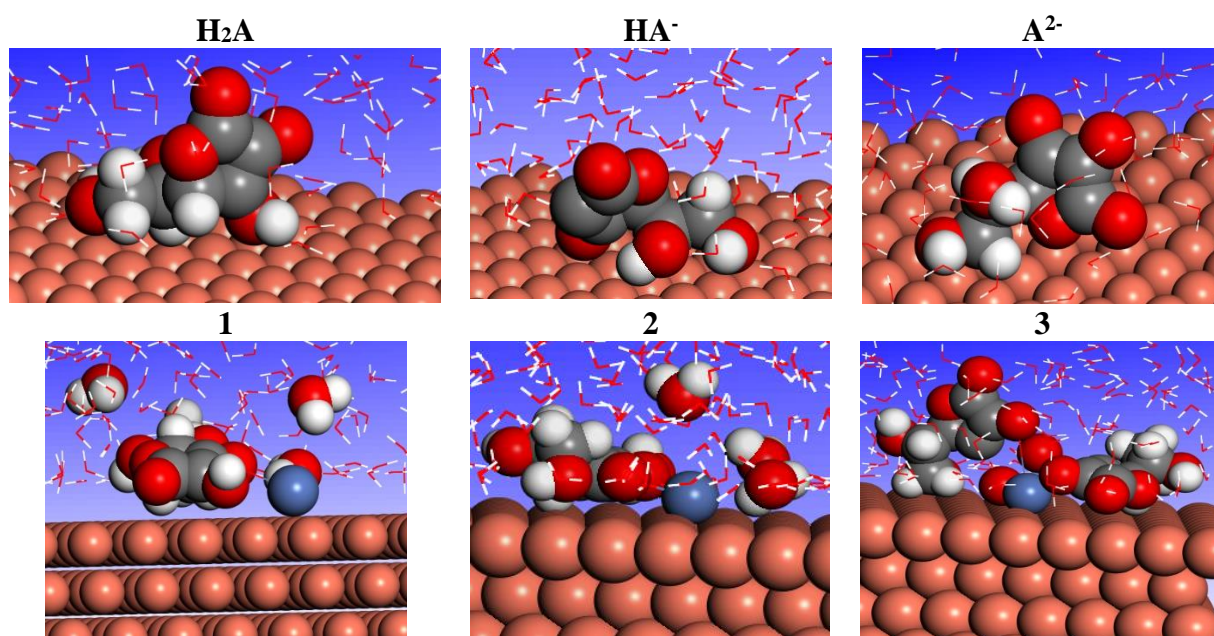


Figure 13. The best adsorption mode of H₂A, HA⁻, A²⁻ and complexes 1, 2 & 3 on the copper(111) surface.

Table 8. Monte Carlo descriptors of Cu(111)/Ni-Asc1/2 NaCl/200 H₂O complexes. All values are in kcal/mol.

Compound	Total energy ($\times 10^3$)	Adsorption energy ($\times 10^3$)	Rigid adsorption energy ($\times 10^3$)	Deformation energy	dE_{ad}/dN_i
H ₂ A	-2.41	-2.43	-2.57	141.50	-82.12
HA	-2.43	-2.42	-2.57	43.01	-68.93
A	-2.38	-6.34	-2.55	-3.79	-3983.62
1	-2.48	-2.75	-2.64	-118.02	-442.01
2	-2.52	-2.73	-2.64	-87.15	-402.68

3	-2.41	-9.53	-2.60	-6.94	-7.21
4	-2.16	-3.52	-2.24	-1.28	-1500.02
5	-2.49	-2.49	-2.64	154.52	-200.64
6	-2.33	-2.35	-2.48	130.01	-128.49

For example, vinyl oxygens of A^{2-} are the closest to the surface. For H_2A , only one of the vinyl hydroxyl groups is close to the surface so it can only be used as monodentate, in agreement with the previous study [26]. On the other hand, the adsorption modes of 1, 2 & 3 complexes are exhibited in Fig. 13 as a representative example. The adsorption of complexes on the surface led to the dissociation of all coordinated waters due to the high affinity of the Ni^{2+} center towards the copper surface. For this reason, the Ni-ion is the closest atom to the surface and the remaining of the complex tends to be parallel to the metal surface.

Table 8 presents the adsorption descriptors of the possible forms of L-Ascorbic acid and their Ni-complexes. Among these descriptors, the adsorption energy is the most relevant energy parameter that describes the nature of adsorption. This parameter is the sum of the rigid adsorption energy and deformation energy before and after the relaxation of adsorbates on the surface, respectively. According to Table 8, all values of adsorption energies are negative indicating that *in-situ* adsorption of all species around the copper electrode can occur spontaneously. Except in the case of A^{2-} and 3, the value of adsorption energy of the other species is comparable, indicating that they are adsorbed simultaneously. The strongest absorption is that of complex 3 (-9.53×10^3 kcal/mol) followed by the deprotonated form of ascorbic acid, A^{2-} (-6.34×10^3 kcal/mol) which uses its bidentate to attach to the Cu-surface.

3.12. Corrosion behavior

For simplicity, before discussing the results derived from the electrochemical corrosion studies performed on the prepared Ni coatings and their interpretation, it is important to recall that the Ni coating electrochemically formed in the Watts bath in the absence of Asc acid is assigned here as (Ni coating)₀, while those formed in the presence of 0.3 M and 0.4 M Asc acid are named as (Ni coating)₁ and (Ni coating)₂, respectively.

3.13. Uniform corrosion studies

Fig. 14 presents the cathodic and anodic polarization curves of the three prepared Ni coatings, namely (Ni coating)₀, (Ni coating)₁, and (Ni coating)₂ in 3.5 wt% NaCl solution at a potential scan rate of 5 mV s^{-1} at room temperature.

It follows from Fig. 14 that ongoing from (Ni coating)₀ to (Ni coating)₂, the current associated with both the cathodic and anodic polarization plots decreases, and the corrosion potential (E_{corr}) is drifted towards the less negative values. In addition, the current density accompanying the anodic polarization curves is markedly reduced, whereas the cathodic curves are slightly biased towards lower

currents. Such results suggest that the anodic processes are inhibited more effectively than the cathodic ones.

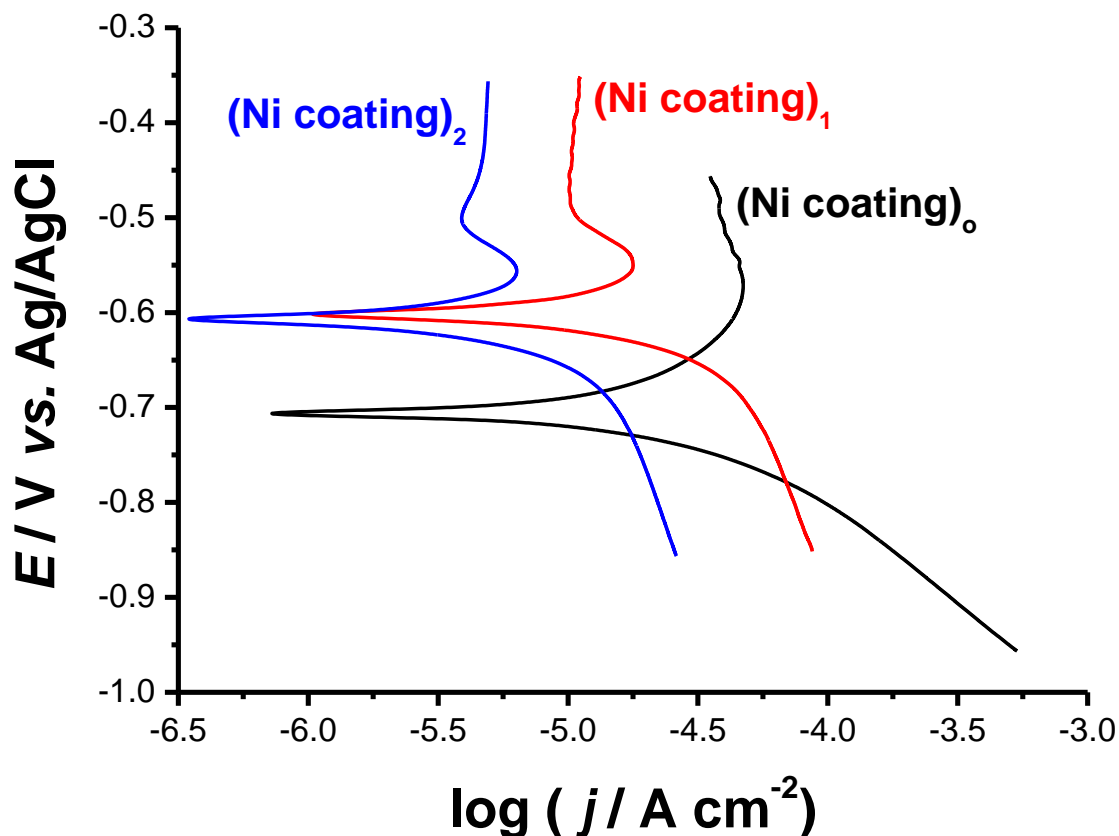


Figure 14. Cathodic and anodic polarization curves of the three prepared Ni coatings in 3.5 wt% NaCl solution at a potential scan rate of 5 mV s^{-1} at room temperature.

Further examination of the cathodic and anodic polarization curves revealed that, in all cases, a typical Tafel response (linear E - $\log j$ relationship) is displayed by the cathodic curves, whereas the anodic ones contravene such a Tafel behavior. The absence of the linear E - $\log j$ relationship on the anodic polarization curves can be attributed to corrosion product deposition and/or passivation. The cathodic polarization curves' Tafel region makes it possible to make a precise evaluation of the cathodic Tafel slope (β_c), and hence the rate of the uniform corrosion in terms of corrosion current density (j_{corr}), via the Tafel extrapolation method. However, the anodic Tafel slope (β_a) values, estimated from the software, are expected to be inaccurate as a result of the lack of the Tafel response on the anodic domains [51-56].

The estimated β_c values are higher than anticipated. The Ni coating formed in the absence of Asc acid, namely (Ni coating)₀ recorded a high β_c value of -219 mV dec^{-1} for the cathodic processes (i.e., the reduction of both water molecules and dissolved O_2 occurring on its surface) in 3.5 wt.% NaCl solution. The value of β_c is significantly increased, referring to a considerably reduced rate of the cathodic

processes (and hence outstanding corrosion resistance for the overall uniform corrosion rate), for the two Ni coatings formed in the presence of Asc, (Ni coating)₁ and (Ni coating)₂. It reached a value of -680 mV dec^{-1} for (Ni coating)₁, and further increased to -760 mV dec^{-1} in the case of (Ni coating)₂. Analogous data were formerly reported by M. Metikos-Hukovic *et al.* [57] who applied some organic additives to effectively control the perchloric acid corrosion of Al. High β_c values ($235\text{-}245 \text{ mV dec}^{-1}$) were estimated during that study [57]. High Tafel slope values are commonly considered irregular as such high Tafel slopes cannot be prophesied for any mechanism [57]. The higher values of β_c were attributed by Metikos-Hukovic and his coworkers [57] to the Al passivity that occurs instantaneously forming a virtually stable ineffectual passive layer, which restricts the reduction capacity of Al [58]. This, in turn, slows any reduction process occurring at the surface by influencing the energy of the double-layer reaction, by introducing a barrier to the transfer of the charge through the film or both [59]. A consistent way of describing the high Tafel slopes was the barrier-film model for the observed HER [59].

The extremely high β_c values, namely -680 mV and -760 mV dec^{-1} recorded for (Ni coating)₁ and (Ni coating)₂ gave corrosion current density (j_{corr}) values, calculated from the Tafel extrapolation method, 3.7×10^{-5} and $1.26 \times 10^{-5} \text{ A cm}^{-2}$ for (Ni coating)₁ and (Ni coating)₂, respectively, not too far from that measured for (Ni coating)₀, $3.85 \times 10^{-5} \text{ A cm}^{-2}$, despite the significant reduction in the cathodic and anodic polarization plots' current densities upon the addition of Asc acid.

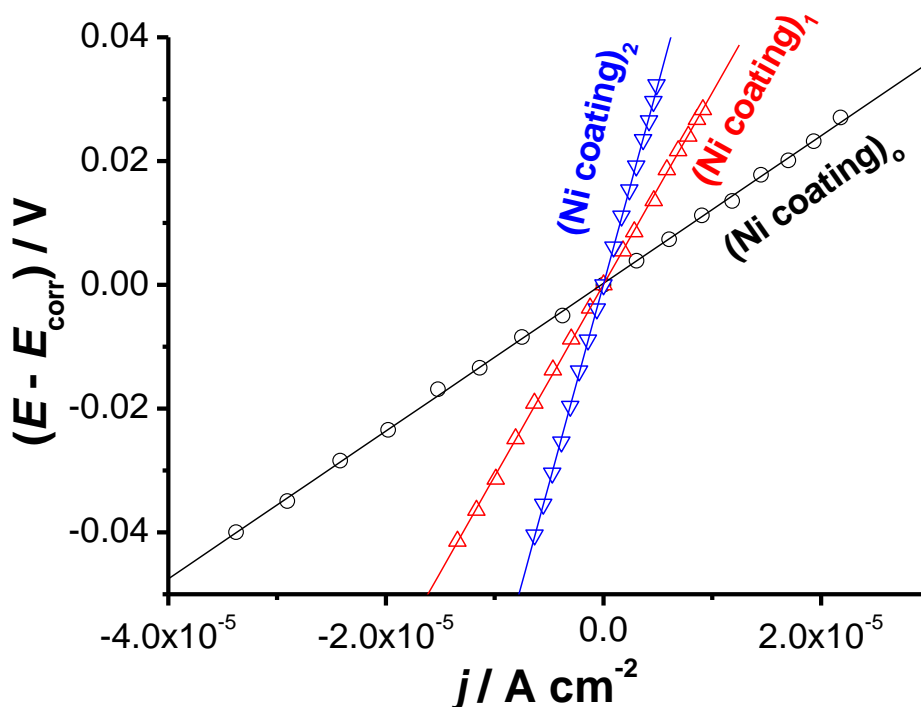


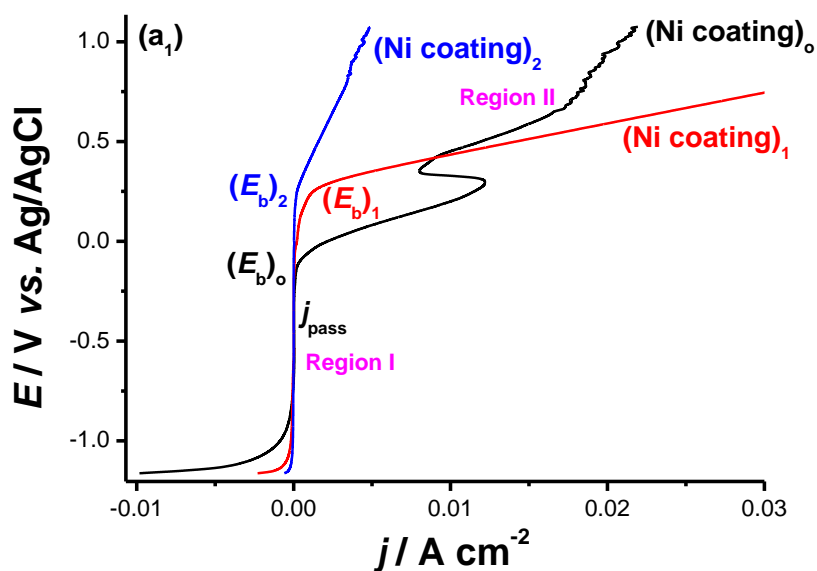
Figure 15. Linear polarization resistance (LPR) plots were recorded for the three prepared Ni coatings in 3.5 wt% NaCl solution at a potential scan rate of 5 mV s^{-1} at room temperature.

To clarify and further assess the high uniform corrosion resistance of (Ni coating)₁ and (Ni coating)₂ versus (Ni coating)₀, linear polarization resistance (LPR) plots were constructed (Fig. 15). The slopes of such linear plots define the polarization resistance R_p (the polarization curve's tangent at E_{corr}) [62]. The value of R_p significantly increased, corresponding to enhanced corrosion resistance, from 1193 $\Omega \text{ cm}^2$ for (Ni coating)₀ to 3096 and 6452 $\Omega \text{ cm}^2$ for (Ni coating)₁ and (Ni coating)₂, respectively. These findings add another evidence of the outstanding uniform corrosion resistance of (Ni coating)₂ in NaCl solutions.

3.14. Anodic behavior (passivity and breakdown of passivity)

Both (Ni coating)₁ and (Ni coating)₂ also exhibited a pronounced inhibitive impact on the anodic behavior, in terms of passivity and passivity breakdown, of the Ni coating in NaCl solutions, as shown in Fig. 16. Upon polarizing the working electrode anodically, the cathodic current density diminishes steadily attaining its zero value at the corrosion potential (E_{corr}). The location of E_{corr} is well-defined in the corresponding logarithmic scale, Fig. 16(a₂).

Owing to passivation, the polarization curves lack active dissolution near E_{corr} . With a reduced passive current (j_{pass}), the Ni coating's passivity (region I) persists up to a particular potential (specified as the breakdown potential, E_b), where the passive layer is locally destroyed forming pits. Under the influence of the electric field applied to the Ni coating's passive oxide film/NaCl_(aq) interface, the aggressive Cl^- anions adsorb on the oxide/electrolyte interface. This adsorption, which occurs preferentially at the passive layer's active sites (defects and defective regions) [61] and competes with the dissolved O_2 , H_2O molecules passivating species adsorption, causes passivity breakdown and initiation of pitting corrosion [62-64].



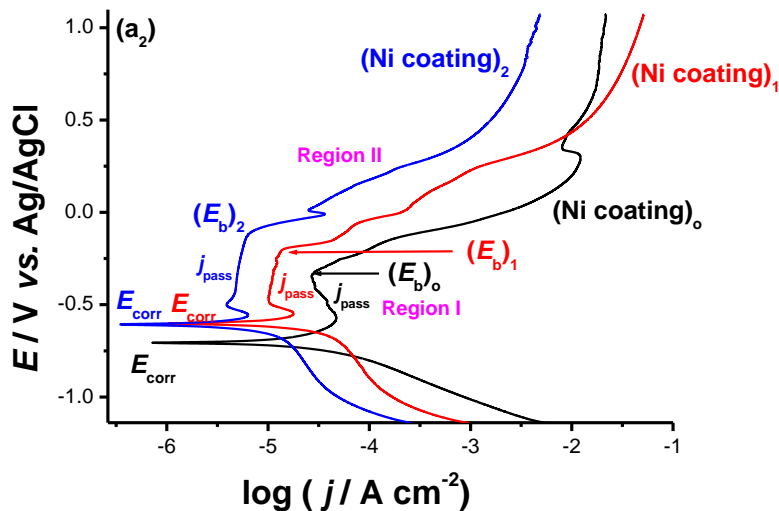


Figure 16: Potentiodynamic anodic polarization curves, in the linear (a₁) and logarithmic (a₂) scales, measured for the three prepared Ni coatings in 3.5 wt% NaCl solution at a potential scan rate of 5 mV s⁻¹ at room temperature.

Once adsorbed, a chemical reaction takes place within the passive oxide film between metal cations and adsorbed Cl⁻ anions [65]. The product of that chemical reaction, namely soluble M-Cl species, leaves the lattice of the passive oxide film to the solution, causing the oxide film to become thinner and dissolve locally [63-66].

Once the applied anodic potential reaches E_b , the passive oxide film is dissolved locally and pits nucleate. Beyond E_b , pits initiate and propagate turning the medium locally acidic [62, 63] thus enabling efficacious local dissolution of the passive oxide film and subsequent pits' growth and propagation [62-65]. This significantly enhanced j_{pass} denotes pit initiation and growth (region II).

The value of j_{pass} is always smaller for (Ni coating)₁ and (Ni coating)₂ than that of (Ni coating)₀. This decrease in j_{pass} is quite obvious in Fig. 16(a₂). The diminished j_{pass} value refers to a strengthened passive layer (a passive layer with increased resistance to pitting corrosion), most probably as a result of the adsorbed Asc molecules which not only altered the texture of the formed Ni coatings as evidenced from XRD analysis (revisit Fig. 9), but also yielded more fine grains as shown by SEM observation (Fig. 10).

Local dissolution of the base metal is retarded at this stage, and hence pitting corrosion rate diminishes. For the adsorbed Cl⁻ to overcome that protective Ni coating barrier and restart pitting, the applied anodic potential must be increased to values higher than $(E_b)_0$, the breakdown potential recorded for the (Ni coating)₀, to invigorate dissolution at the less favorable sites. Increasing the concentration of Asc (C_{Asc}) in the Watts bath from 0.3 M to form (Ni coating)₁ to 0.4 M, where (Ni coating)₂ is yielded, is proved to improve the coating's characteristics and protectiveness against corrosion. This in turn leads to a greater presence of the less favorable sites for Cl⁻ adsorption. Dissolution processes would therefore be delayed until increasingly greater potentials are achieved. This may explain why the (Ni coating)₂'s E_b value is nobler than that of (Ni coating)₁. These results mean that the presence of Asc acid in the

plating bath endows the formed Ni coatings with improved characteristics and high resistance against both uniform and corrosion processes in NaCl solutions

4. CONCLUSIONS

Ascorbic (Asc) acid as an environmentally friendly additive for Ni electrodeposition from Watts bath has been inspected. Evaluation of the results led to the inference of the following conclusions:

- The addition of Asc acid to the nickel bath of the Watts type resulted in a significant change in the polarization plots towards more negative potential values and thus inhibits the reduction rate of Ni²⁺ ions.
- The adsorption of Asc acid on the cathode surface during nickel electrodeposition follows the Langmuir isotherm.
- The formation of Ni coating occurs under diffusion control *via* a nucleation and growth mechanism.
- The percentage of the throwing power (T.P.%) increased more than 8 times in the plating solution containing 0.4 M Asc acid.
- The microhardness of Asc acid-containing Ni coatings is higher than that of nickel deposited without Asc acid.
- Inclusion of Asc acid into Watts bath permits to modify of the texture of the resulting Ni coatings; In the presence of Asc acid, fine grains are observed on the Ni coatings.
- The prepared Ni coatings in presence of Asc acid exhibited a higher corrosion resistance towards both the uniform and pitting corrosion processes in NaCl solutions than that obtained without Asc acid.
- The DFT and Monte Carlo simulations could successfully explain the real reason behind the retarding of Ni electroplating rate on the copper surface. The findings indicated that the equilibrium deprotonation of L-ascorbic acid and the formation of Ni-ascorbate complexes produce at least nine compounds (3 ligands and 6 Ni-ascorbate complexes) that have a high tendency toward adsorption on the surface.

ACKNOWLEDGMENT

The researchers would like to thank the Deanship of Scientific Research, Qassim University for funding the publication of this project

SUPPORTING INFORMATION:

S1. Electrodeposition of the Ni coating

Electrochemical formation of Ni coating was carried out utilizing a Ni electrolyte of the Watts-type: 0.63 M of nickel sulphate hexahydrate, 0.09 M of nickel chloride hexahydrate and 0.3 M of boric acid in absence and presence of ascorbic acid at pH 3.0 and 27°C for 10 min. The pH was adjusted using

1:1 HCl or NaOH. As a cathode and anode for nickel deposition, Cu and Pt sheets of the same dimensions (2.7×2.7 cm) were respectively utilized. The deposition cell consists of a rectangular trough (10.0 × 3.0 cm) made of transparent plastic. The Cu substrate was cleaned by dipping in the pickling mixture for 1 min before each run, then washed, dried, and put in the balance to weight.

S2. Calculation of the current efficiency

Using a Cu-coulometer, the current efficacy, $F = w_{\text{exp}}/w_{\text{th}}$, was estimated (w_{exp} is the experimental weight of Ni deposit, and w_{th} is the theoretical weight). By utilizing a Haring-Blum cell comprising one anode between two cathodes, the percentage of throwing power (T.P.%) of the solution was measured, where the proportion of the near-to-far distance was 1:5 [33].

S3. Electrochemical characterizations during the electroformation of Ni coating

Using copper substrates, potentiodynamic polarization behavior was traced by scanning the potential at a sweep rate of 5 mVs⁻¹ towards the more significant negative potentials. All the potentials throughout this work were measured using Ag/AgCl as a reference electrode. In a three-compartment cell comprising a Pt working electrode, an Ag/AgCl reference electrode and a Pt sheet counter electrode, the anodic linear stripping voltammetric (ALSV) method was performed. The electrodeposition of nickel for a certain period was accomplished at a fixed potential. Subsequently, in the same plating bath, stripping was achieved soon by scanning the potential in the noble direction. Additionally, at a Pt disc electrode, chronoamperometry (j-t transients) analysis was investigated. Before each run, polishing of the Pt disc electrode with Al₂O₃ powder was performed until a lustrous appearance was attained, then washed with double distilled water. All electrochemical measurements were recorded utilizing 1000 Potentiostat/Galvanostat/ZRA Gamry Instrument.

S4. Electrochemical studies on the corrosion behavior of the Ni coating in NaCl

A standard jacketed three-electrode cell was used for electrochemical measurements. A Pt electrode and a Ag/AgCl electrode were used as auxiliary electrode and reference electrode, respectively. All potentials were measured against Ag/AgCl. Electrochemical experiments were performed *via* connecting the cell to a 1000 Potentiostat/Galvanostat/ZRA Gamry Instrument connected to PC. The solution temperature was set at (25 °C ± 0.2 °C) using a temperature-controlled bath with water circulating through the outer cell jacket.

S4.1. Uniform corrosion studies

Tafel extrapolation and linear polarization resistance (LPR) methods were employed to study the effect of adding ascorbic acid to the Watts bath on the uniform corrosion behavior of the prepared Ni coatings. The working electrode is first stabilized in the test solution for 2 h, then LPR and Tafel

polarization measurements were consecutively conducted. For LPR measurements, the potential of the working electrode is swept from -20 to $+20$ mV versus E_{corr} at an extremely slow scan rate of 0.167 mV s^{-1} starting from more negative potential to the anodic direction. Finally, Tafel polarization measurements were conducted *via* sweeping the potential of the working electrode within the Tafel potential region ($E = E_{\text{corr}} \pm 250$ mV) using a scan rate of 1.0 mV s^{-1} .

S4.2. Anodic behaviour (passivity layer growth and breakdown of passivity)

Potentiodynamic anodic polarization measurements were also conducted to investigate the passive layer growth and its breakdown on the surfaces of the prepared Ni coatings. Measurements were conducted in 3.5 wt.% NaCl solutions at room temperature. The working electrode is first stabilized for 2 h at the rest potential, then scanned linearly from a starting cathodic potential of -2.0 V(SCE) with scan rate 5.0 mV s^{-1} till an ending anodic potential of $+2.0$ V(SCE).

S5. Characterizations

The Vickers micro-hardness of the Ni deposits was assessed using the Tukon Series B200 microhardness tester with a diamond pyramid indenter by indentation technique at 10 mN load. The XRD patterns of the coatings were acquired using an X'Pert Pro diffractometer at 40 mA and 45 kV ($\lambda = 1.5418$ Å, rated as 1.6 kW) with $\text{CuK}\alpha$ radiation. Finally, surface morphology of the nickel deposits was examined using Quanta FEG 250 Scanning electron microscope (FEI Company, Hillsboro, Oregon-USA).

S6. Computational details

S6.1. DFT calculations on isolated molecules

The geometry of the possible Ni-ascorbate complexes was optimized using M06 [67] functional with mixed basis set, where the standard 6-311++G** basis set was used for all atoms except Ni-atom, which was treated by the relativistic compact Stuttgart-Dresden effective core potential [68]. The findings showed that the triplet spin multiplicity of Ni-complexes is favored than the singlet ones. Furthermore, the three forms of L-ascorbic acid (**H₂A**, **HA⁻** and **A²⁻**), **Fig. 1**, were optimized using the M06/6-311++G** model chemistry. The aqueous medium was simulated by the density-based solvation model, SMD [69] as implemented in Gaussian 16 software [70].

S6.2. Monte Carlo simulations

The adsorption of the nine proposed compounds (six Ni-ascorbate complexes + L-ascorbic acid and their deprotonated forms) on the copper surface was studied by Metropolis Monte Carlo simulations [71] using the adsorption locator module, as implemented in Materials Studio 2017 [72]. The surface of

copper (111) has been reported to be the most stable of all facets of copper [73], and thus it has been used to simulate the adsorption process. Simulation box (2.5 × 2.5 × 3.6 nm) with periodic boundary conditions was used for this purpose. Six layers of copper atoms give enough depth to study the interaction molecules with the surface. The electrostatic and van der Waals energetic components of the interaction were calculated using Ewald and atom-based summation method, respectively. COMPASS force field [74] was used to optimize the structures of all components over the surface. To simulate the medium effect, two NaCl and 200 H₂O molecules were loaded with one molecule of Ni-complex or one form of L-ascorbic acid together on the copper surface.

S7. The cartesian coordinates of the M06 optimized geometry of the studied molecules

H ₂ A	HA ⁻
O 1 O 0.79222400 2.32571500 -0.42228700 O 3.08676500 0.52926300 0.55020600 H 3.55217600 -0.29077900 0.76634900 C 0.90586500 0.99147500 -0.37855300 O 2.07229700 -2.16849400 0.19446700 C 1.88463400 0.19718200 0.05293100 O 0.19631100 -1.19253400 -0.61260900 C 1.44678400 -1.18721500 -0.08976700 O -1.33681500 0.31363800 1.35597200 H -0.90630000 1.10319900 1.69320800 O -3.83604600 -0.19871200 0.21982800 H -3.67959200 -0.19489000 1.16928700 C -0.24549000 0.15041000 -0.81565100 H -0.45007300 0.28244800 -1.88869800 C -1.52702200 0.42484800 -0.03848400 H -1.85824500 1.44169100 -0.30684300 C -2.62681700 -0.55064600 -0.39668700 H -2.79568700 -0.53704500 -1.47893900 H -2.30283200 -1.56367800 -0.11681600 H 1.61494700 2.73173800 -0.12489100	O 2 O 0.95175400 2.29207500 -0.41588100 O 3.02762000 0.54073500 0.61042400 C 0.95004100 0.97840300 -0.40860400 O 1.97623300 -2.27864200 0.24534700 C 1.96889500 0.16190200 0.11922300 O 0.22692100 -1.17921100 -0.64165800 C 1.45707500 -1.25464700 -0.04702800 O -1.23672800 0.36613500 1.32717000 H -1.00432200 1.22576700 1.68567400 O -3.77686400 -0.15528600 0.23798100 H -3.63224200 -0.21594600 1.18709500 C -0.20149100 0.16796600 -0.85509500 H -0.40885800 0.29859800 -1.92809900 C -1.47439800 0.46171200 -0.06257600 H -1.80801300 1.47558700 -0.33509600 C -2.58021600 -0.51807000 -0.39390900 H -2.76582800 -0.51436000 -1.47370500 H -2.25305400 -1.52851700 -0.11071000 H 1.80138700 2.58883000 -0.04429400
A ²⁻	Complex 1
O 1 O 1.08722700 2.36844300 -0.37966900 O 2.88095100 0.34892000 0.91054900 C 0.96461500 1.18279600 -0.36418200 O 1.79230200 -2.28605300 0.06478700 C 1.90913000 0.15113800 0.25560500 O 0.26286000 -0.99197300 -0.94647800 C 1.34870400 -1.21180400 -0.16373100 O -0.93098400 0.22964000 1.25916100 H -1.69561000 0.15229100 1.84068800 O -3.53441800 -0.16133900 0.54892100 H -4.19301600 -0.85682700 0.50347100 C -0.18403600 0.37435100 -0.93681900 H -0.41374500 0.66966400 -1.96570200 C -1.39154800 0.52738000 -0.03609700 H -1.71730400 1.58034500 -0.10309300 C -2.53925100 -0.37204800 -0.43058200 H -2.89251900 -0.10201100 -1.43756300 H -2.19700500 -1.41544500 -0.44113900	1 3 O -2.52326700 1.59206800 -0.27869900 C -1.39587100 2.36259300 -0.08181600 C -0.28666000 1.44387000 -0.04901300 C -0.67471900 0.16059000 -0.18923600 O 0.11970200 -0.87778700 -0.17941200 O 1.06863800 1.76550000 0.07889600 C -2.17545200 0.18052800 -0.39166200 H -2.44463700 -0.14769000 -1.39878200 O -1.40544300 3.55841300 0.05149300 C -3.01728100 -0.60369200 0.62532600 H -2.70102800 -0.32037700 1.64124500 C -2.86351200 -2.11509000 0.45396900 H -3.47919400 -2.60650900 1.21612400 H -1.82244500 -2.40547300 0.60408500 O -4.39193600 -0.31818200 0.43413500 H -4.52566800 0.63753200 0.44232200 O -3.21613000 -2.54350300 -0.85139900 H -4.15701500 -2.37068300 -0.97612400 O 1.86480100 -0.59207200 2.08915300 H 2.33272200 -0.09286700 2.76985400 H 0.96228500 -0.74590900 2.39838200 O 2.04490000 -0.16114400 -2.09684100 H 1.16728400 -0.42258500 -2.41245400 H 2.31298300 0.60991700 -2.61268700

	O 3.96776100 0.49483600 0.29510700 H 4.34209400 1.36529700 0.11566700 H 4.66611300 -0.16102600 0.17222000 O 2.91127200 -2.10133400 -0.13884600 H 2.80542300 -2.54315800 -0.99188900 H 2.64800500 -2.73569600 0.54103400 H 1.17309400 2.63254500 0.49658100 Ni 1.98852100 -0.20716000 0.02001100
Complex 2	Complex 3
O 3 O -2.33009500 1.66207200 -0.33305200 C -1.11753500 2.33869400 -0.10499000 C -0.07162600 1.33081500 -0.06119400 C -0.61825600 0.09726400 -0.24177700 O 0.08171900 -1.01959000 -0.25097300 O 1.26360300 1.51840600 0.12115500 C -2.10330500 0.23538500 -0.43506600 H -2.42272600 -0.08575100 -1.43150600 O -1.09516300 3.53656700 0.01339200 C -2.97828300 -0.45426100 0.61928400 H -2.57453700 -0.21500300 1.61411200 C -3.03017300 -1.97082000 0.45546800 H -3.57326900 -2.39327900 1.31119600 H -2.01759900 -2.37612900 0.44479300 O -4.32571900 0.00632600 0.51715900 H -4.29572300 0.96567300 0.40686100 O -3.64542600 -2.35426700 -0.76791400 H -4.48932100 -1.88716200 -0.80892100 O 1.95908200 0.00671800 2.15506100 H 1.56811200 0.86856700 1.87690400 H 1.30936300 -0.44728800 2.70324100 O 2.25178500 0.31587500 -2.04040600 H 1.60025600 -0.02227600 -2.66639400 H 1.88673100 1.16160500 -1.69585100 O 4.04115200 0.07552900 0.27911100 H 4.14649100 0.32456300 1.20695200 H 4.34041400 0.82378600 -0.25124100 O 2.33975700 -2.47840900 -0.08085800 H 1.44819000 -2.76628100 -0.33117400 H 2.96616600 -2.87552100 -0.69511300 Ni 1.97489200 -0.38184900 0.00087100	-2 3 O 4.56448900 1.37806300 -0.08172500 C 3.64066300 1.92510800 -1.04711800 C 2.40127800 1.21026900 -0.91026800 C 2.53409000 0.25064900 0.06772500 O 1.59314800 -0.57631200 0.38429100 O 1.26012100 1.33748600 -1.58424200 C 3.92359000 0.30795100 0.64434900 H 3.92992600 0.56905800 1.70954700 O 4.03905300 2.82580600 -1.76059100 C 4.74865800 -0.96683600 0.42050700 H 4.53715000 -1.33914700 -0.58947700 C 4.45004200 -2.06892500 1.43371200 H 4.87072700 -3.01671400 1.06742700 H 3.36935500 -2.17827000 1.54016700 O 6.15632200 -0.66858500 0.53198600 H 6.24245700 0.22234000 0.15921400 O 5.00073500 -1.76099700 2.71696000 H 5.83544800 -1.31257400 2.52357300 O -4.56457000 -1.37794700 -0.08177000 C -3.64066900 -1.92524600 -1.04694800 C -2.40128700 -1.21038400 -0.91017900 C -2.53405700 -0.25074900 0.06780600 O -1.59307900 0.57617100 0.38436900 O -1.26016900 -1.33759000 -1.58422000 C -3.92358800 -0.30792700 0.64436700 H -3.93001500 -0.56906500 1.70955600 O -4.03923200 -2.82563600 -1.76071200 C -4.74850700 0.96695400 0.42051800 H -4.53684200 1.33931100 -0.58941600 C -4.44990800 2.06894200 1.43383300 H -4.87037300 3.01681400 1.06751300 H -3.36922400 2.17810200 1.54050300 O -6.15621100 0.66882500 0.53182200 H -6.24238800 -0.22205800 0.15896200 O -5.00091900 1.76104500 2.71695400 H -5.83568900 1.31280500 2.52338100 Ni 0.00000500 -0.00007300 -0.83699200
Complex 4	Complex 5
-4 3 O 5.61342900 -1.40124300 -0.44549300 C 5.19676700 -2.47657000 0.40830400 C 3.75321800 -2.46191400 0.56501200 C 3.25122300 -1.36699300 -0.19826800 O 2.08859800 -0.92003300 -0.39194600 O 3.09142400 -3.31122200 1.28593500 C 4.44072100 -0.66668100 -0.84725300 H 4.38006500 -0.70340400 -1.94185800 O 6.08381700 -3.20579200 0.84593000 C 4.59967600 0.79601700 -0.38698200 H 4.25636600 0.88157200 0.64857100 C 3.82968100 1.78969000 -1.25390700 H 3.75111900 2.74933100 -0.72736100 H 2.82476600 1.40792900 -1.43965400 O 6.00408100 1.17407700 -0.45415200 H 6.46181300 0.33179200 -0.29353200 O 4.49970100 1.98781400 -2.51432400	-4 3 O 4.34841100 -2.71023000 1.96687100 C 3.13962900 -1.99526800 2.19063500 C 2.58629400 -1.54808200 0.90550100 C 3.49726200 -1.96168800 -0.11153500 O 3.47202000 -1.78721000 -1.36108300 O 1.47856100 -0.90015400 0.82202500 C 4.63586700 -2.72906900 0.55469800 H 4.65229100 -3.77423100 0.22855600 O 2.76610100 -1.87060100 3.34015600 C 6.03966000 -2.11251400 0.35571400 H 5.93782200 -1.01892300 0.33361600 C 6.74345600 -2.55330300 -0.92365500 H 7.67417000 -1.97690600 -1.03067000 H 6.09296100 -2.36200400 -1.77747200 O 6.90401000 -2.48542500 1.44778300 H 6.30897400 -2.56665500 2.20937300 O 7.06341700 -3.94796900 -0.92323300

<p>H 5.43593900 1.89452700 -2.28762700 Ni 0.01903800 -0.84151900 0.40889200 O 0.09582400 4.01858800 1.17463800 C 0.48854400 2.96486000 2.11600900 C 0.36667300 1.69791700 1.45407400 C -0.09501200 1.91879500 0.15712800 O -0.34544300 1.00630600 -0.70403700 O 0.59996200 0.48768000 1.91735700 C -0.31046200 3.39860100 -0.05755200 H 0.31114500 3.80447100 -0.86822500 O 0.82818000 3.34628900 3.23157200 C -1.78306100 3.77159600 -0.30156900 H -2.40843500 3.12082800 0.31863900 C -2.21904100 3.64731300 -1.75991700 H -3.31660200 3.61505200 -1.81330800 H -1.81682900 2.72078600 -2.17394200 O -2.00269200 5.15409500 0.09081500 H -1.37602800 5.26030600 0.82833200 O -1.74178000 4.75751800 -2.54003500 H -1.69110600 5.47961600 -1.89656800 O -4.29791800 -2.93566600 -0.97267100 C -2.98296900 -3.15807900 -1.56098300 C -2.02522000 -2.38564800 -0.83320800 C -2.68301600 -1.68187600 0.17397600 O -2.13251500 -0.87883100 0.99777000 O -0.71078700 -2.29704600 -1.00906200 C -4.16363600 -2.01414400 0.12567500 H -4.50122100 -2.52247000 1.03807700 O -2.94337900 -3.93022600 -2.51643100 C -5.07681300 -0.80427600 -0.15362300 H -4.53189900 -0.11131400 -0.80685500 C -5.50505100 -0.04856600 1.10241200 H -5.92143200 0.92600500 0.80490200 H -4.63127800 0.11714700 1.73494800 O -6.28463500 -1.22971800 -0.82349700 H -5.99861100 -2.01540800 -1.31915700 O -6.48161100 -0.76231500 1.86868400 H -7.12091500 -1.09940500 1.22372900 O 0.44772900 -2.77918200 1.35510600 H 0.13655300 -3.12081400 0.49244500 H 1.43432400 -2.94302600 1.36422700</p>	<p>H 7.57292000 -4.09946200 -0.11480100 O 0.53146300 5.16585100 -1.60881200 C 0.82888000 3.81313200 -2.04479600 C 0.23068900 2.86553700 -1.13526600 C -0.44554200 3.58286600 -0.13791600 O -1.12256900 3.21104600 0.87838700 O 0.33233300 1.55835700 -1.30632400 C -0.24346400 5.06817300 -0.40876900 H -1.20323700 5.57870400 -0.57230600 O 1.49423400 3.70794400 -3.06427300 C 0.53705400 5.78562100 0.70534800 H 1.32309200 5.10932200 1.05972700 C -0.32570600 6.21912200 1.88890200 H 0.31802400 6.41971800 2.75870800 H -1.01633500 5.40881000 2.12924100 O 1.15510500 6.98672800 0.17105200 H 1.35075000 6.73171400 -0.74746100 O -1.07685600 7.40526900 1.57809700 H -0.52006200 7.86189800 0.93025500 O -4.48025700 -3.68243600 -0.60122700 C -3.17398700 -3.38252900 -1.17316200 C -2.64610500 -2.17536600 -0.56943600 C -3.59870300 -1.69861100 0.34659400 O -3.62698700 -0.66348800 1.09380200 O -1.49230900 -1.65412000 -0.93203400 C -4.78831100 -2.64776600 0.33696100 H -4.94640000 -3.10585000 1.32373700 O -2.77657700 -4.15752300 -2.02614500 C -6.08966500 -1.97024000 -0.13074900 H -5.83564000 -1.25397000 -0.92038300 C -6.84937700 -1.24513200 0.97858000 H -7.56206500 -0.53466900 0.53204500 H -6.13085900 -0.69732000 1.59078200 O -6.99000800 -2.97088400 -0.67588200 H -6.37154500 -3.62852100 -1.04230300 O -7.57012900 -2.17242100 1.80727400 H -7.75685900 -2.91135400 1.20920800 O 1.07957900 -0.70196100 -2.22647500 H 1.95280100 -1.05746600 -1.94412100 H 1.16629300 0.27252900 -2.28792100 O -1.17215800 0.49447800 1.15285300 H -2.09822900 0.14457200 1.13500800 H -1.20271300 1.48014400 1.06563900 Ni -0.09688700 -0.30397800 -0.43203100</p>
Complex 6	
<p>-4 3 O 1.48151100 4.43784500 1.44229800 C 1.00419300 3.37323500 2.32141700 C 0.82324100 2.18740900 1.53131100 C 1.17344700 2.47360300 0.22094300 O 1.12220900 1.63022100 -0.75151700 O 0.39614700 0.99163800 1.89182900 C 1.58571400 3.91709100 0.10435400 H 2.62672300 4.03470900 -0.22789700 O 0.85834500 3.67046000 3.49920600 C 0.65994700 4.75348800 -0.79356400 H -0.36945400 4.41565100 -0.63453800 C 0.99613900 4.65974800 -2.27986100 H 0.14144000 5.01765400 -2.87085800 H 1.19220400 3.61702400 -2.53603800 O 0.76385400 6.15444400 -0.42410700 H 0.91105000 6.11068700 0.53586500 O 2.15646100 5.44638300 -2.59960100 H 2.12512100 6.17012400 -1.95731200 O -4.90503100 -0.14377400 -1.07263100 C -3.56888100 0.26238800 -0.95054000 C -2.85965500 -0.66069800 -0.03107600 C -3.84346600 -1.62307000 0.44998900 O -3.72143300 -2.54352200 1.26643500 O -1.63745000 -0.58452700 0.26682700 C -5.16533700 -1.32538200 -0.27248200</p>	

H -5.42348200 -2.13697600 -0.95931000	
O -3.19827200 1.24113500 -1.55508700	
C -6.38202900 -1.03222400 0.63891500	
H -6.01937600 -0.50950200 1.53823300	
C -7.11629000 -2.28567400 1.11899400	
H -7.93872100 -1.97612100 1.77467200	
H -6.41303000 -2.89025000 1.69665700	
O -7.32348700 -0.19549500 -0.04150500	
H -6.79607400 0.36573500 -0.62632100	
O -7.63698800 -3.09797900 0.06884800	
H -8.56405600 -2.85383800 -0.07542800	
O 3.96534600 -3.20274600 -1.60264200	
C 2.61025400 -2.98157700 -2.11808900	
C 1.95666600 -2.04080900 -1.25380300	
C 2.83027700 -1.68684600 -0.23605800	
O 2.53724400 -0.88554000 0.72198700	
O 0.72989600 -1.55446700 -1.30416900	
C 4.13848900 -2.41799000 -0.41012900	
H 4.98548400 -1.73564700 -0.56732900	
O 2.31161500 -3.60581400 -3.12525500	
C 4.46175700 -3.38622000 0.73923300	
H 3.52461800 -3.84789500 1.07009900	
C 5.14414000 -2.72040800 1.93245200	
H 5.06104100 -3.37441900 2.81321000	
H 4.64482800 -1.77325100 2.14586300	
O 5.35641300 -4.42512100 0.26392900	
H 5.08221300 -4.53201500 -0.66355400	
O 6.53132300 -2.46766300 1.66173800	
H 6.77644500 -3.17187500 1.04404900	
Ni 0.55213500 -0.16607100 0.19197300	

References

1. G. G. Gawrilov, Chemical (Electroless) Nickel Plating, Portcullis Press Ltd., (1979), Redhill, Surrey, UK.
2. G. A. Di Bari , “Electrodeposition of Nickel” in Modern Electroplating, M. Schlesinger & M. Paunovic, (Eds.), Wiley & Sons, (2000) New Jersey pp. 139.
3. W. Blum, and G. B. Hogaboom, Principles of Electroplating and Electroforming, McGraw-Hill, (1949) New York.
4. O. A. Taranina, N. V. Evreinova, I. A. Shoshina, V. N. Naraev, and K. I. Tikhonov, *Russ. J. Appl. Chem.*, 83(1) (2010) 58.
5. N. V. Sotskaya, and O. V. Dolgikh, *Prot. Met.*, 44(5) (2008) 479.
6. E. Rudnik, M. Wojnicki, and G. Wloch, *Surf. Coat. Technol.*, 207 (2012) 375.
7. L. Lee, W. Chung, U. Jung, and Y. Kim, *Surf. Coat. Technol.*, 205 (2011) 4018.
8. N. F. El Borae, and M. A. M. Ibrahim, *Surf. Coat. Technol.*, 347 (2018) 113.
9. M. A. El Sayed, and M. A. M. Ibrahim, *Int. J. Electrochem. Sci.*, 14 (2019) 4957.
10. M. A. M. Ibrahim, and R. M. Al Radadi, *Int. J. Electrochem. Sci.*, 10 (2015) 4946.
11. M. A. M. Ibrahim, S. S. Abd El Rehim, S. M. Abd El Wahaab, and M. M. Dankeria, *Plat. Surf. Finish.*, 86 (1999) 69.
12. M. A. M. Ibrahim, *J. Appl. Electrochem.*, 36 (2006) 295.
13. J. K. Dennis, T. E. Such, Nickel and Chromium Plating, Wiley, 1972.
14. U. S. Mohanty, B.C. Tripathy, P. Singh, and S.C. Das, *J. Appl. Electrochem.*, 31(2001) 969.
15. E. A. Pavlatou, M. Raptakis, and N. Spyrellis, *Surf. Coat. Technol.*, 201(2007) 4571.
16. U. S. Mohanty, B. C. Tripathy, S. C. Das, and V. N. Misra, *Metall Mater. Trans. B*, 36B (2005) 737.
17. T. Osaka, T. Sawaguchi, F. Mizutanic, T. Yokoshima, M. Takai, and Y. Okinakab, *J. Electrochem. Soc.*, 146 (1999) 3295.

18. R. Riastuti, S. T. Siallagan, A. Rifki, F. Herdino, and C. Ramadini, *Mater. Sci. Eng.*, 541 (2019) 012053.
19. S.M.H.Z Shirazi, M. E. Bahrololoom, and M. H. Shariat, *Surf. Eng. Appl. Electrochem.*, 52 (2016) 434.
20. B.-Wei Wang, C.-Ying Lee, and H.-Bin Lee, *Surf. Coat. Technol.*, 337 (2018) 232.
21. M. A. M. Ibrahim, and S. N. Alamri, *J. Appl. Surf. Fin.*, 2 (2007) 332.
22. C. Zhang, H. Liu, P. Ju, L. Zhu, and W. Li, *J. Electrochem. Soc.*, 165 (11) (2018) D518.
23. A. J. Cobley, and D. R. Gabe, *Trans IMF*, 84(3) (2006)149.
24. H.-Ling Sun, C.-Chann Shiue, and S.-Jen Jane Tsai, *J. Anal. At. Spectrom.*, 16 (2001) 838.
25. Y. Jinku, Z. Lili, S. Hui, W. Yuehua, Y. Meiqi, L. Hongliang, X. Zhefeng, and K. Matsugi, *Rare Met. Mater. Eng.*, 47(2) (2018) 0436.
26. D. Cesario, E. Furia, G. Mazzone, A. Beneduci, G. De Luca, and E. Sicilia, *J. Phys. Chem. A.*, 121 (2017) 9773.
27. S. Mahata, I. Mitra, S. Mukherjee, V. Pera Reddy, GKr. Ghosh, W. Linert, and S. C. Moi, *Afr. J. Chem.*, 72 (2019) 229.
28. R. Oukhrib, Y. Abdellaoui, A. Berisha, H. Abou Oualid, J. Halili, K.Jusufi, M A El Had, H. Bourzi, S. El Issami, F. A. Asmary, V.S. Parmar, and C. Len, *Sci. Rep.*, 11 (2021) 3771.
29. Z.Z. Tasić, M. B. P. Mihajlović, A.T. Simonović, M. B. Radovanović, and M. M. Antonijević, *Sci. Rep.*, 9(2019) 1.
30. R. P. Oliveira, D. C. Bertagnolli, E. A. Ferreira, L. Da Silva, and A. S. Paula, *Surf. Coat. Technol.*, 349 (2018) 874.
31. J. W. Dini, *Electrodeposition-The material science of coatings and substrates*, Noyes Publications, (1993) New Jersey, pp. 194.
32. M. Abdullah, *Corros. Sci.*, 44 (2002) 717.
33. M. A. M. Ibrahim, *J. Chem. Technol. Biotechnol.*, 75 (2000) 745.
34. G. Trejo, A F Gil, I Gonzalez, *J. Appl. Electrochem.*, 26 (1996)1287.
35. E. Gileadi , E. Kirowa-Eisner E, J. Penciner, *Interfacial Electrochemistry An Experimental Approach*, Addison-Wesley Inc., Reading, MA, 1975.
36. T. Degen, M. Sadki, E. Bron, U. König, and G. Nénert, *The High Score suite. Powder Diffraction Powder Diffraction* 29(S2): S13-S18, 2014.
37. B. D. Cullity, S. R. Stock, *Elements of X-Ray Diffraction*, 3rd Ed., Prentice-Hall Inc., 2001, p 96-102, ISBN 0-201-61091-4.
38. R. Jenkins, R. L. Snyder, *Introduction to X-ray Powder Diffractometry*, John Wiley & Sons Inc., 1996, p 89-91, ISBN 0-471-51339-3.
39. M. A. M. Ibrahim, F. T. Al-Wadanni, and O. Al-Jaldi, *Prod. Finish.*, 76 (12) (2012) 1.
40. M. A. M. Ibrahim, F. Kooli, and N. Alamri, *Int. J. Electrochem. Sci.*, 8 (2013)12308.
41. A. Szymanski, J. M. Szymanski, *Hardness Estimation of Minerals, Rocks and Ceramic Materials*, New York-Tokyo, (1989) PWN-Polish Scientific Publisher.
42. A. Iost, G. Guillemot, Y. Rudermann, and M. Bigerelle, *Thin Solid Films*, 524 (2012) 229.
43. N. O. Eddy, B. I. Ita, and QSAR, *J. Mol. Model*, 17 (2011) 359.
44. L. C. Murulana, A. K. Singh, S K Shukla, M. M. Kabanda, and E. E. Ebenso, *Ind. Eng. Chem. Res.*, 51(2012) 13282.
45. T. Peme, L. O. Olasunkanmi, I. Bahadur I, A. S. Adekunle, M. M. Kabanda, and E. E. Ebenso, *Molecules*, 20 (2015)16004.
46. M. Dibetsoe, L. O. Olasunkanmi, O. E. Fayemi, S. Yesudass, B. Ramaganthan, I. Bahadur, A.S. Adekunle, M.M. Kabanda, and E. E. Ebenso, *Molecules*, 20 (2015) 15701.
47. H Tanak, A Ağar, M Yavuz, *J. Mol. Model.*, 16 (2010) 577.
48. L. O. Olasunkanmi, I. B. Obot, M. M. Kabanda, and E. E. Ebenso, *J. Phys. Chem. C.*, 119 (2015) 16004.
49. R G Pearson, *Inorg. Chem.*, 27(1988) 734.

50. N. A. Wazzan, *J. Ind. Eng. Chem.*, 26 (2015) 291.
51. H. J. Flitt, and D. P. Schweinsberg, *Corros. Sci.*, 47 (2005) 2125.
52. H. J. Flitt, and D. P. Schweinsberg, *Corros. Sci.*, 47 (2005) 3034.
53. F. Mansfeld, *Corros. Sci.*, 47 (2005) 3178.
54. B. Rosborg, J. Pan, and C. Leygraf, *Corros. Sci.*, 47(2005) 3267.
55. E. McCafferty, *Corros. Sci.*, 47 (2005) 3202.
56. M A Amin, K F Khaled, and S A Fadel-Allah, *Corros. Sci.*, 52 (2010) 140.
57. M. Metikos-Hukovic, Z. Grubac, and E. Stupnisek-Lisac, *Corrosion*, 50 (1994)146.
58. W. Li, T. Cochell, and A. Manthiram, *Sci. Rep.*, 3 (2013)1.
59. A. K. Vigh, Oxide Films: influence of solid-state properties on electrochemical behavior, in: J.W. Diggle (Ed.), oxide and oxide films, Vol. 2 Marcel Dekker, Inc New York NY, 1972 pp. 1-92.
60. F. Mansfeld, *Corrosion*, 37(1981) 301.
61. J. A. Richardson, and G. C. Wood, *Corros. Sci.*, 10 (1970) 313.
62. A. Kolics, J. C. Polkinghorne, and A. Wieckowski, *Electrochim. Acta*, 43(1998) 2605.
63. Z. A. Foroulis, and M. J. Thubrikar, *J. Electrochem. Soc.*, 122 (1975) 1296.
64. R. T. Foley, and T. H. Nguyen, *J. Electrochem. Soc.*, 129 (1982) 464.
65. T. P. Hoar, *Corros. Sci.*, 7(1967) 341.
66. Z. Szklarska-Smialowska, Pitting Corrosion of Metals. NACE Houston TX, 1986.
67. Y. Zhao, D. G. Truhlar, *Theor. Chem. Acc.* 120 (2008) 215.
68. D. Andrae, U. Hußermann, M. Dolg, H. Stoll, H. Preuß, *Theor. Chim. Acta* 77 (1990) 123.
69. A. V. Marenich, C. J. Cramer, D. G. Truhlar, *J. Phys. Chem. B*, 113 (2009) 6378.
70. M. Frisch, et al., Gaussian 16 Rev. B. 01, Wallingford, CT. 2016.
71. N. Metropolis, A.W. Rosenbluth, M. N. Rosenbluth, A.H. Teller, E.J. Teller, *J. Chem. Phys.* 21 (1953) 1087.
72. Dassault Systèmes BIOVIA, Materials Studio, 17.1.0.48, San Diego: Dassault Systèmes, 2017.
73. L. Xu, J. Lin, Y. Bai, M. Mavrikakis, *Top. Catal.* 61 (2018) 736.
74. H. Sun, P. Ren, J. R. Fried, *Comput. Theor. Polym. Sci.* 8 (1998) 229.

© 2022 The Authors. Published by ESG (www.electrochemsci.org). This article is an open access article distributed under the terms and conditions of the Creative Commons Attribution license (<http://creativecommons.org/licenses/by/4.0/>).